THE JOURNAL OF PHYSICAL CHEMISTRY C
A JOURNAL OF THE AMERICAN CHEMICAL SOCIETY

pubs.acs.org/JPCC
Article

CO Oxidation over Platinum Nanoclusters: Unraveling the Role of the Cluster Size and the Supporting Surface

Mina Taleblou, Matteo Farnesi Camellone, Stefano Fabris, and Simone Piccinin*

Cite This: J. Phys. Chem. C 2023, 127, 21132−21149
Read Online

ACCESS | Metrics & More | Article Recommendations

ABSTRACT: The present work focuses on the catalytic activity of Pt nanoclusters as well as single-atom Pt catalysts supported by TiO_2 and Co_3O_4. We performed an extensive set of calculations based on density functional theory to investigate the CO oxidation reaction on Pt clusters supported on TiO_2 and Co_3O_4 surfaces. We identified the catalytic active sites at the interface between the supported metal and the metal oxide substrate, and we determined different oxidation reaction pathways, proceeding either through the Langmuir−Hinshelwood (LH) or Mars-van Krevelen (MvK) mechanisms. Comparing clusters of different sizes, our calculations suggest that the Pt_1/TiO_2 catalyst, where Pt is present as an adatom or substituting a Ti site, is the most active catalyst for CO oxidation. We find that the kinetics of the reaction on Pt nanoclusters is highly dependent on the size of the metal cluster but does not follow a well-defined trend. Moreover, the kinetics of the reaction is remarkably influenced by the type of supporting metal oxides.

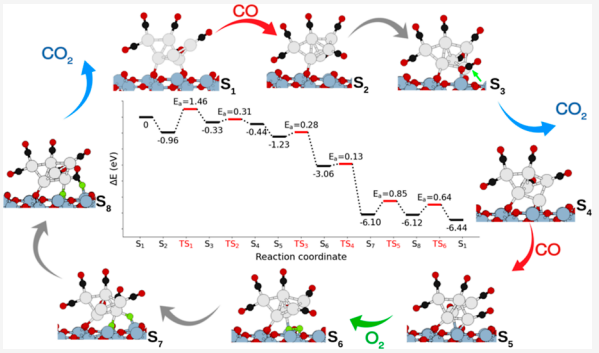

INTRODUCTION

CO oxidation represents one of the most investigated reactions in the field of surface science, and heterogeneous catalysis is essential for lowering automotive emissions and cleaning air. Small metallic clusters and metallic nanoparticles (NPs) of noble metals such as Au,[1−3] Pd,[4] Ir,[5] Cu,[6] Ag,[7] and Pt[8] supported on different metal or metal/oxide surfaces have shown to enhance the conversion of CO into CO_2. The activity of metallic NPs supported by metal or metal/oxide catalysts is controlled by various factors: particle size,[9,10] nature of the support,[11,12] temperature,[13] and the shape and chemical composition of the particle.[14] Several theoretical and experimental studies have been performed to investigate and improve the catalytic properties of metal-supported catalysts.[3,15−20]

In particular, metal-oxide-supported Pt catalysts have attracted great interest because of their exceptional catalytic activity for a large number of oxidation reactions including low-temperature CO oxidation.[8,16,21−27] Reducible oxides (such as CeO_2, TiO_2, and Co_3O_4) represent very active catalytic supports where Pt NPs are deposited or Pt atoms are dispersed as single-atom catalysts (SACs). However, despite extensive theoretical and experimental studies, the origin of the high catalytic activity of Pt/oxide catalysts has not been clarified. A clear understanding of the nature of the active sites, the role played by the size of Pt-supported NPs, and the coordination of Pt single atoms is lacking and are still under debate. Recently, CO oxidation promoted by Pt_x ($4 \leq x \leq 35$) nanoclusters supported on the (110) rutile TiO_2 surface has been investigated in a combined experimental and theoretical work.[28] The study shows the existence of a correlation between the amount of CO_2 produced and the number of Pt atoms located at the edge of the first layer of the supported Pt nanoclusters, suggesting that the interface between supported clusters and the substrate plays a crucial role in the oxidation of CO. Similar conclusions have been reported for Pt-supported clusters on anatase (101) and magnetite $Fe_3O_4(001)$ surfaces.[29] SACs with atomically distributed metal centers that maximize the utilization of supported metals have attracted great attention in catalysis.[30,31] It has been shown by experiments and theory that SACs efficiently promote the conversion of CO to CO_2.[32−35]

In this work, we present an extensive density functional theory (DFT)-based investigation of the reaction mechanisms by which the Pt/TiO_2 and Pt/Co_3O_4 systems catalyze the CO oxidation as a function of the size of supported Pt nanoclusters. Brookite, the least investigated among the polymorphs of TiO_2, has been the subject of recent experimental works aimed

Received: August 24, 2023
Revised: October 4, 2023
Accepted: October 9, 2023
Published: October 20, 2023

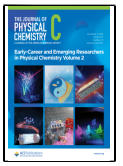

https://doi.org/10.1021/acs.jpcc.3c05714
J. Phys. Chem. C 2023, 127, 21132−21149

at obtaining crystals with well-defined surface terminations.[36,37] We will focus in particular on the (210) surface, which has been predicted to be the most stable facet.[38] In the case of Co_3O_4, we will focus on the Co-terminated (111) facet, which has been the subject of intensive experimental and theoretical works.[39,40] We have considered two different mechanisms: the Mars-van Krevelen (MvK) and Langmuir−Hinshelwood (LH) mechanisms. Our calculations show that CO oxidation takes place at the Pt−metal oxide interface via both the MvK and LH mechanisms.

COMPUTATIONAL DETAILS

DFT calculations discussed in this work have been performed with the Quantum ESPRESSO package,[41] using pseudopotentials to describe the ions and adopting a plane wave basis set to expand the Kohn−Sham wave functions. We adopted the Perdew−Burke−Ernzerhof generalized gradient approximation exchange−correlation functional.[42] Brookite TiO_2(210) and Co_3O_4(111) surfaces[40] were modeled by the DFT + U approach using Hubbard U terms of 3.5 and 3.0 eV acting on d orbitals of Ti and Co atoms, respectively. The value of Hubbard correction U for Co_3O_4 is based on our previous work on this system[40] where we investigated the structural and electronic properties of Co_3O_4 as a function of U. In the case of TiO_2, most of the theoretical works present in the literature adopt a value in the range of 2.5−4.5 eV.[43] We decided to adopt an intermediate value of 3.5 eV. We used a projector augmented wave pseudopotential for oxygen atoms and ultrasoft pseudopotentials for all the other atoms. All calculations were spin-polarized. The Brillouin zone was sampled at the gamma point, and the electronic occupations were smeared by the Marzari−Vanderbilt scheme with a width of 0.136 eV (0.01 Ry). Energy cutoffs of 30 and 300 Ry were applied to the wave function and augmentation charge density, respectively.

To model the TiO_2(210) surface, we used a stoichiometric slab, including four Ti layers. To model the polar Co_3O_4(111) surface, we employed a symmetric, nonstoichiometric slab, in analogy to our previous works on this system,[40] including a total of 11 layers. The bottom two layers of the slabs were held fixed, while the other layers were allowed to relax. We included 12 Å of vacuum in the direction normal to the surface to avoid spurious interactions among periodic replicas of the systems. In the present work, we considered Pt_1, Pt_4, and Pt_6 clusters. The optimized structures of the supported Pt clusters were obtained using the genetic algorithm. Further details on the structural models can be found in our previous work on this subject.[44]

We define the adsorption energy of CO molecules (E_{ads}^{CO}) as

$$E_{ads}^{CO} = [E(n\mathrm{CO@Pt/support}) - E(\mathrm{Pt/support}) - nE(\mathrm{CO})]/n \quad (1)$$

where $E(n\mathrm{CO@Pt}_x\mathrm{/support})$, $E(\mathrm{Pt}_x\mathrm{/support})$, and $nE(\mathrm{CO})$ are the total energies of the combined system $n\mathrm{CO/Pt}_x$/support, the Pt_x/support system, and CO molecules in the gas, respectively, and n is the number of CO adsorbates on the system.

To evaluate the effects of temperature and pressure on the energetics of the systems, we employed the ab initio thermodynamics framework.[45] The gas-phase species i (i = O_2 or CO) are assumed to behave as ideal gases, i.e. their chemical potentials μ_i depend on the temperature (T) and pressure (p) according to the expression

$$\mu_i(T, p) = \mu_i(T, p^\circ) + k_B T \ln\left(\frac{p_i}{p^\circ}\right) \quad (2)$$

where p° is the standard pressure (1 bar), p_i is the partial pressure of species i, and k_B is the Boltzmann constant. The values of μ_i at p° and different temperatures were acquired from the JANAF thermochemical tables.[46] A change in the chemical potential of O_2 or CO at a finite pressure with respect to its value at zero temperature is defined as

$$\Delta\mu_i(T, p) = \mu_i(T, p) - E_{tot,i} \quad (3)$$

where $E_{tot,i}$ is the DFT total energy of molecular oxygen or CO in the gas phase.

The Gibbs free energy of formation as a function of the chemical potential can be approximated as below

$$\Delta G(T, p) = G(\mathrm{Pt}_x\mathrm{O}_y n\mathrm{CO/surf}) - G(\mathrm{Pt}_x\mathrm{/surf}) - y\mu_O(T, p) - n\mu_{CO}(T, p) \quad (4)$$

$$\simeq \mathrm{E}(\mathrm{Pt}_x\mathrm{O}_y n\mathrm{CO/surf}) - \mathrm{E}(\mathrm{Pt}_x\mathrm{/surf}) - \mathrm{y}\left(\frac{1}{2}\mathrm{E}(\mathrm{O}_2) + \Delta\mu_O(\mathrm{T, p})\right) - n(\mathrm{E(CO)} + \Delta\mu_{CO}(\mathrm{T, p})) \quad (5)$$

$$= E_{form}(\mathrm{Pt}_x\mathrm{O}_y n\mathrm{CO/surf}) - y\Delta\mu_O(T, p) - \mathrm{n}\Delta\mu_{CO}(T, p) \quad (6)$$

where $E(\mathrm{Pt}_x)$/surf and $E(\mathrm{Pt}_x\mathrm{O}_y)$/surf are the total energies of metallic (Pt_x) and oxidized ($\mathrm{Pt}_x\mathrm{O}_y$) clusters supported on the oxide surfaces, respectively. In this formulation, the Gibbs free energy of the systems is approximated to the DFT total energy.

The formation energy of an oxygen vacancy (FE_{O_v}) is calculated as[47]

$$FE_{O_v} = \mathrm{E}(\mathrm{O_v@system}) + \frac{1}{2}\mathrm{E}(\mathrm{O}_2) - \mathrm{E(system)} \quad (7)$$

where $E(\mathrm{O_v@system})$ and $E(\mathrm{system})$ represent the total energies of the system under investigation with and without an oxygen vacancy, respectively.

To model the CO oxidation mechanisms, locate the transition states, and determine the activation energies of the elementary steps, we used the climbing image nudged elastic band method (CI-NEB).[48] A minimum number of 9 images were considered for different paths, and the reaction paths were optimized until the forces were less than 0.05 eV/Å. Selected examples of the NEB input files for both the MvK and LH oxidation mechanisms are available at the following link: 10.5281/zenodo.8278565.

RESULTS AND DISCUSSION

Adsorption of CO on Supported Metallic Pt_x Clusters. As a first step in studying CO oxidation, we investigated how CO molecules interact with the catalyst. Since a strong interaction and the resulting CO poisoning could impair the Pt NP catalysts,[49] there have been efforts to study and control the adsorption of CO on Pt systems.[50−52] The strength of CO adsorption depends on the adsorption site[53,54] and surface

https://doi.org/10.1021/acs.jpcc.3c05714
J. Phys. Chem. C 2023, 127, 21132−21149

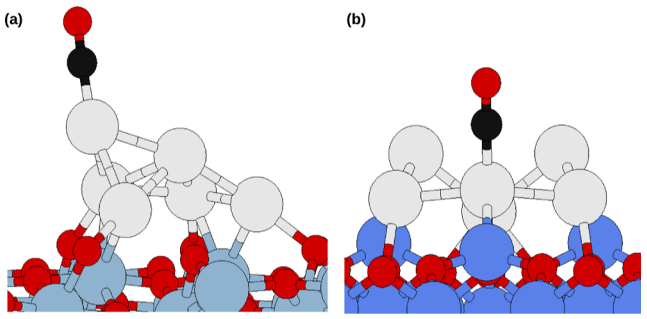

Figure 1. Structures of the most stable adsorption sites for a single CO molecule adsorbed on metallic Pt_6 supported on (a) TiO_2 and (b) Co_3O_4 surfaces.

strain[55] on bulk Pt, as well as the particle size and CO coverage on Pt NPs.[52,56]

We first considered CO adsorption on metallic Pt_6 and Pt_1 catalysts anchored on TiO_2 and Co_3O_4 as well as metallic Pt_4 anchored on TiO_2. The most favorable site for the adsorption of a single CO molecule was found to be the top site of the Pt_6-supported cluster. The adsorption energy of a single CO molecule, E_{ads}^{CO}, in its most favorable site on Pt_6 was found to be −2.30 and −2.55 eV on TiO_2 and Co_3O_4, respectively (see Figure 1a,b). These findings are in agreement with previous studies[50] and suggest that the interaction of CO with supported Pt nanoclusters is stronger compared to bulk Pt, where the CO adsorption energy is within the range −1.22 to −1.66 eV, depending on the adsorption site.[55]

Next, we investigated the effect of coverage on the adsorption of CO molecules on the Pt_6/TiO_2 and Pt_6/Co_3O_4 nanocatalysts. Figure 2 shows a plot of the average CO adsorption energies as a function of CO coverage. It is clear from Figure 2 that the interaction between the CO molecules and the supported Pt_6 metallic clusters decreases when increasing the coverage, implying that the molecules repel each other. When full CO coverage is reached (one CO molecule per Pt atom), the average adsorption energies for CO adsorption on Pt_6/TiO_2 and Pt_6/Co_3O_4 are −1.85 and −1.79 eV, respectively. This is in agreement with the results of a previous work on the Pt/Al_2O_3 catalyst, where a similar weakening of the CO−Pt interaction at increasing CO coverage has been observed.[57]

In addition, our calculations prove that these small Pt-supported clusters can easily adopt different configurations to facilitate the adsorption of the CO molecules. Indeed, the adsorption of molecular CO induces significant modifications in the structure and morphology of the supported clusters, see Figure 3a,b.

In the case of the Pt_6/TiO_2 system, upon increasing the coverage of CO molecules adsorbed on the Pt_6 cluster, some Pt−O bonds at the interface between the Pt cluster and the TiO_2 support break, as shown in Figure 3a. This does not happen in the case of the Pt_6/Co_3O_4 system due to a stronger interaction between the supported Pt_6 cluster and the Co_3O_4 surface, see Figure 3b. Similar modifications in the structure and morphology of supported metallic clusters induced by the adsorption of CO molecules have been observed on the Pt/Al_2O_3[58] and Au_x/CeO_2 catalysts.[59] A different behavior has been observed for Pt clusters supported on Fe_2O_3. Here, the interaction between CO molecules and the support stabilizes Pt dimers against dissociation into atomic Pt and induces agglomeration of Pt atoms into small clusters.[52]

We also considered the interaction between CO molecules and smaller Pt clusters supported on TiO_2 and Co_3O_4 surfaces. The computed average adsorption energies for CO adsorption are found to be −2.13 eV on Pt_4/TiO_2 and −2.28 (−2.08) eV on Pt_1/TiO_2 (Pt_1/Co_3O_4), suggesting a stronger adsorption of CO on smaller Pt systems.

In the present work, we focused on the CO adsorption on the most stable structure for each of the supported Pt clusters, identified in our previous work via global optimization through the genetic algorithm combined with DFT calculations.[44] As shown in that work, there can be several isomers close in energy to but structurally distinct from the global minimum. At a finite temperature, the Pt clusters could therefore interconvert between these different isomers (fluxionality). While we did not explore the effects of this phenomenon, previous works have addressed this topic.[60,61] In particular, the relation between the Pt clusters activity and their morphology was investigated in detail for the case of the dehydrogenation of ethylene.[62] Here, on the other hand, we limited ourselves to investigating the effects of cluster size and catalyst support starting from the global minimum for each system.

Ab Initio Thermodynamics. As a first step to model the thermodynamic stability of Pt clusters under the reaction conditions, we have used the ab initio thermodynamics approach to obtain the phase diagram of supported metallic Pt_x clusters in a CO-only atmosphere.

Looking first at metallic Pt_6 clusters, the Gibbs free energies of formation on the two supports are reported in Figure 4 as a function of the CO chemical potential, $\Delta\mu_{CO}$. The range of

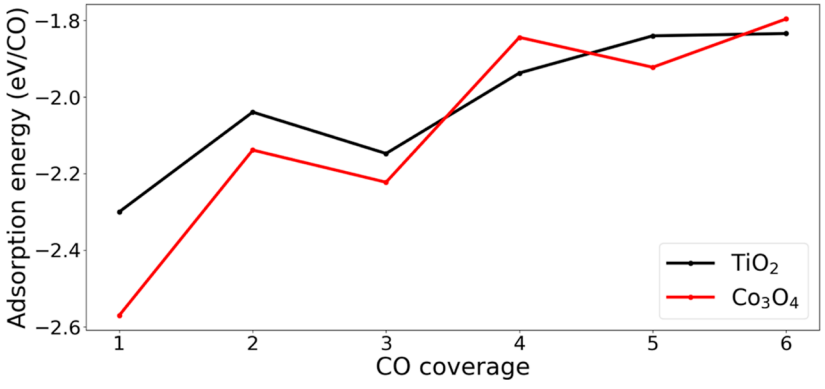

Figure 2. Average adsorption energy of CO molecules on the Pt_6 cluster as a function of CO coverage normalized by the number of CO molecules.

https://doi.org/10.1021/acs.jpcc.3c05714
J. Phys. Chem. C 2023, 127, 21132−21149

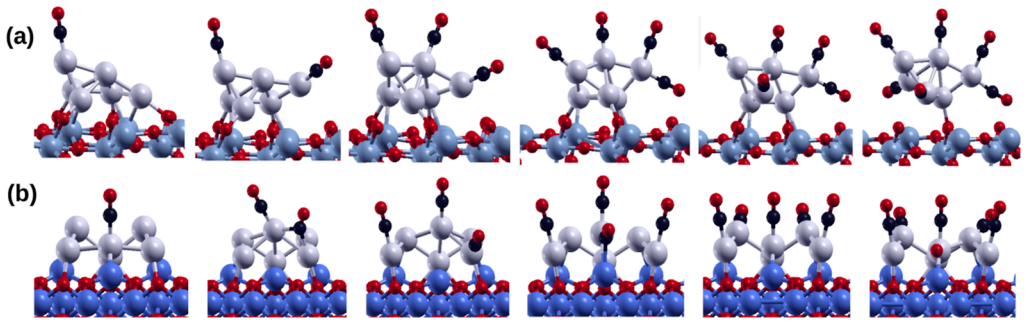

Figure 3. Cluster deformation under different coverages of CO for Pt_6 supported on (a) TiO_2 and (b) Co_3O_4.

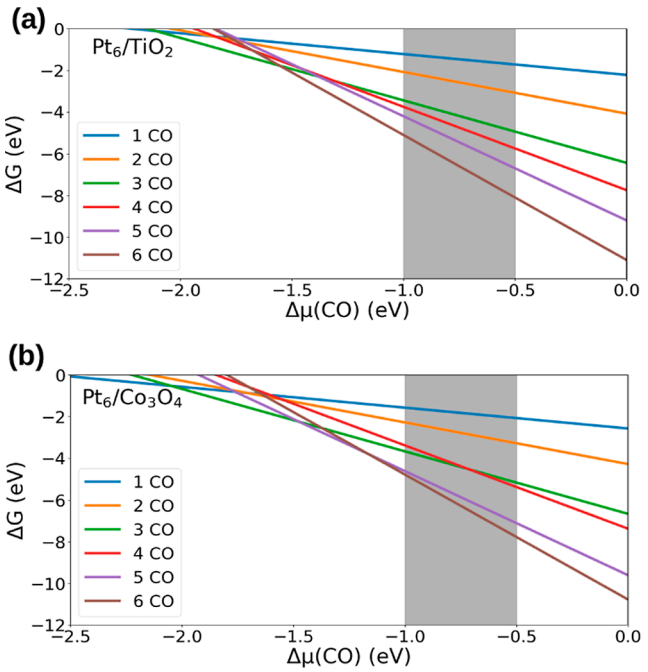

Figure 4. Different coverages of CO on (a) Pt_6/TiO_2 and (b) Pt_6/Co_3O_4 systems. $\Delta G = 0$ corresponds to the metallic systems. The right side of the plot correlates to the lower temperature and higher CO pressure and vice versa.

$\Delta\mu_{CO}$ we are interested in varies from −1.0 to −0.5 eV, corresponding to the experimental catalytic conditions of temperature in the 300−500 K range and CO pressure in the 0.2−0.8 bar range. It is clear from Figure 4 that within the above-mentioned range of $\Delta\mu_{CO}$, our calculations predict that metallic Pt_6 clusters are fully covered by CO molecules regardless of the type of support. This result is in line with previous theoretical[63] and experimental studies.[64]

Next, we will consider the effects of an atmosphere in which both oxygen and CO are present. In our recent work, we have studied the oxidation of metallic Pt clusters supported on TiO_2 brookite and $Co_3O_4(111)$ surfaces.[44] When exposed to an oxygen-only atmosphere, the clusters were found to be partially oxidized over a large range of oxygen chemical potentials. To consider the effects of both oxygen and CO in the atmosphere, we employ the formalism of constrained ab initio thermodynamics[65] to compute the Gibbs free energy of formation of the metal- and oxide-supported Pt nanocatalysts decorated with varying amounts of CO molecules.

We therefore performed a series of structural optimizations, varying both the oxygen content of the Pt clusters and the coverage of the CO molecules. With a high oxygen content and a high CO coverage, structural optimizations often led to the spontaneous formation and desorption of some CO_2 molecules. These combinations of oxygen content and CO coverage are therefore unlikely to be present under the steady-state conditions we are interested in modeling and will therefore not be included in the phase diagram discussed below. The resulting phase diagrams for Pt_6 on TiO_2 and Co_3O_4 are displayed in Figure 5.

The ranges of $\Delta\mu_{CO}$ and $\Delta\mu_O$ in which we are interested in are $-0.5 < \Delta\mu_{CO} \leftarrow 1$ eV and $0 < \Delta\mu_O < -0.5$ eV (see cyan squares in Figure 5), corresponding to experimental conditions of $300 < T < 500$ K and $0.1 < p_{O_2,CO} < 1$ bar. As shown in

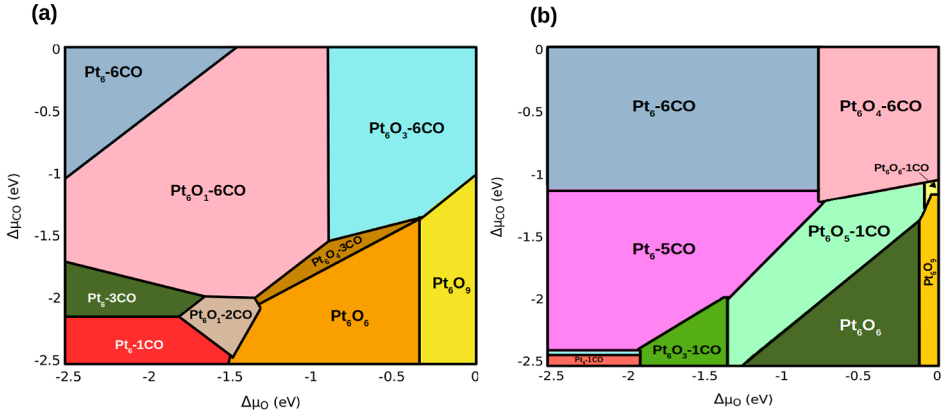

Figure 5. Phase diagram of Pt_6O_x/CO_y supported on (a) Co_3O_4 and (b) TiO_2, with x being the number of oxygen and y denoting the number of CO molecules, in thermodynamic equilibrium with gas-phase O_2 and CO.

https://doi.org/10.1021/acs.jpcc.3c05714
J. Phys. Chem. C 2023, 127, 21132−21149

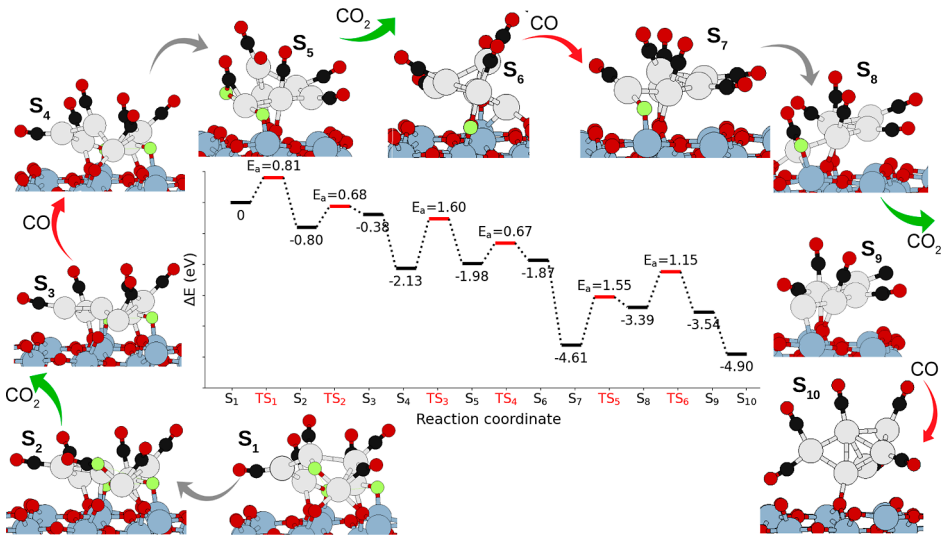

Figure 6. Reaction between adsorbed CO and atomic oxygen atoms of a partially oxidized Pt cluster.

Table 1. Values of FE_{O_v} Calculated for TiO_2 and Co_3O_4 Surfaces in the Absence and Presence of Pt Clusters

system	FE_{O_v} (eV)	system	FE_{O_v} (eV)
TiO_2 surface	3.9−5.2	Co_3O_4 surface	1.9−2.1
Pt_6/TiO_2/6CO	3.0−4.9	Pt_6/Co_3O_4/6CO	1.9−2.5
Pt_4/TiO_2/4CO	2.9−4.4	Pt_4/Co_3O_4/4CO	
Pt_1/TiO_2/1CO	2.1−4.1	Pt_1/Co_3O_4/1CO	1.3

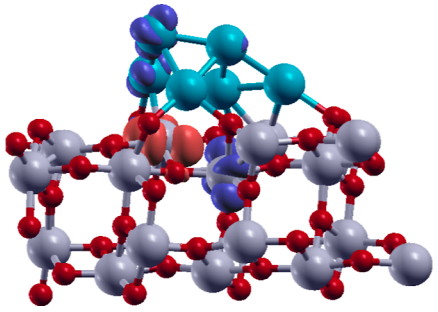

Figure 7. Spin density of the Pt_6/TiO_2 system in the presence of an O vacancy.

Figure 5, within the above-mentioned ranges of $\Delta\mu_{CO}$ and $\Delta\mu_O$, the thermodynamically most stable structures are Pt_6O_4/Co_3O_4 and Pt_6O_3/TiO_2 fully covered with CO molecules.

Our calculations therefore suggest that under experimental conditions, metallic Pt clusters are partially oxidized and fully decorated by CO molecules, regardless of the type of support.

CO Oxidation on Supported PtO_x Clusters. In the previous section, we have shown that, under experimental conditions of temperature and pressure ($300 < T < 500$ K and $0.1 < p_{O_2,CO} < 1$ bar), the Pt_6 cluster supported on brookite is partially oxidized to Pt_6O_3. In the following, we focus on the reactivity of the Pt_6O_3 cluster supported on TiO_2 toward CO oxidation. The minimum energy paths and the transition states for the elementary steps have been identified using the NEB algorithm and are shown in Figure 6. Here, we assume that the source of oxygen for the conversion of CO to CO_2 is the O atoms belonging to the oxidized Pt_6O_3 cluster (in Figure 6, the O atoms of the Pt cluster are highlighted by green color). Here and in the following, the energy of each step is reported relative to the initial step (S1), and the activation energy of step $S_n \rightarrow S_{n+1}$ is reported relative to the energy of S_n. For product desorption, the final state was constructed by placing the product sufficiently far from the catalyst so that it interacts weakly. The reaction energy for desorption steps was computed with the product in the gas phase to ensure there is no interaction between the product and the catalyst. When the CI-NEB did not identify a transition state for the desorption step, we report only the reaction energy for this step, i.e., the negative adsorption energy of the product.

The predicted reaction path for CO oxidation involves two steps: the oxidation of a CO molecule followed by the desorption of the resulting CO_2 molecule. As shown in Figure 6, the activation energies for the formation of the first CO_2 molecule and its desorption from the cluster are 0.81 and 0.68 eV, respectively. Once CO_2 has desorbed, either a gas-phase CO molecule or a gas-phase O_2 molecule can bind to the free sites. The adsorption energy of CO is −1.75 eV, while the adsorption energy of O_2 is −0.88 eV. We therefore consider the adsorption of CO as the most likely next step. This suggests that the reoxidation of the cluster is unfavorable compared to a reaction that leads to complete reduction of the Pt_6O_3 cluster. We therefore computed the activation energies for the formation and desorption of a second CO_2 molecule, 1.60 and 0.67 eV, respectively, while the barriers for forming and desorbing a third CO_2 molecule are 1.55 and 1.15 eV, respectively. As a result of this process, we end up with a metallic Pt cluster fully decorated with CO molecules. Further calculations show that this structure does not bind O_2 molecules, inhibiting the reoxidation of the cluster. In light of these findings, in the next sections, we will focus on the reactivity of metallic Pt clusters supported on both TiO_2 and $Co_3O_4(111)$.

CO Oxidation on Supported Pt_x Clusters. Most previous theoretical works on CO oxidation on supported metallic clusters focused on two competing reaction mechanisms: MvK andLH mechanisms. The MvK mechanism involves the oxidation of CO by surface O atoms of the support, whereas in the LH mechanism, both reactants (CO and O) are chemisorbed on the catalyst.

In the case of a nonreducible support like Al_2O_3, a combined theoretical and experimental work has shown that, for Pt

https://doi.org/10.1021/acs.jpcc.3c05714
J. Phys. Chem. C 2023, 127, 21132−21149

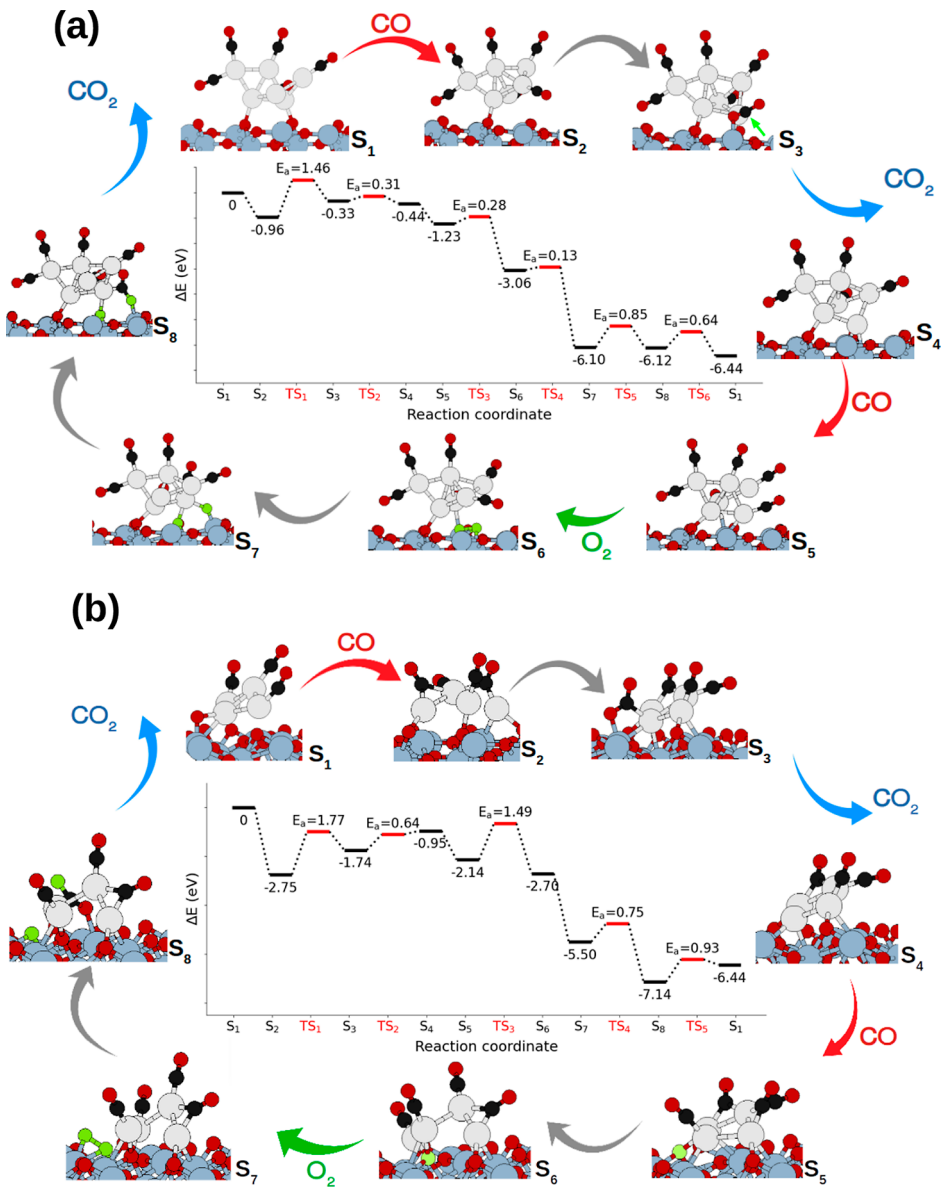

Figure 8. Energy diagrams for CO oxidation via MvK oxidation mechanism on (a) TiO_2/Pt_6 and (b) TiO_2/Pt_4 catalysts. Here, E_a is the activation energy to go from the step S_i to S_{i+1}.

clusters with diameters in the 1.2−20 nm range, measured turnover rates and activation energies were essentially independent of the cluster size, and the kinetically relevant step was assigned to the dissociation of O_2, assisted by adsorbed CO.[8] For small clusters, however, a recent work[66] on Pt_x/Al_2O_3 has revealed a strong dependence of the turnover rate on size, for clusters containing up to 35 atoms.

In the case of reducible supports, where the O vacancies can play a mechanistic role, several works have considered the MvK mechanism as well. For example, Beniya et al.[66] performed experiments on mass-selected clusters deposited on TiO_2, showing that both the LH and MvK mechanisms are active, with the LH being dominant. Thang and Pacchioni[29] used DFT calculations to propose a MvK mechanism for CO oxidation on Pt_4/TiO_2 anatase. In the case of Pt clusters supported on CeO_2, Liu et al.[67] proposed a MvK mechanism involving Pt atoms at the interface between CeO_2 and the Pt cluster as the active site.

It is therefore clear that on the basis of previous works in the literature, both the LH and MvK mechanisms need to be considered in order to provide a comprehensive picture of CO oxidation on supported Pt clusters.

MvK Mechanisms on Supported Pt Clusters. *Creation of Oxygen Vacancies.* First, we focus on the MvK mechanism, where the oxidation of CO is promoted by lattice O atoms at the interface between the supported Pt clusters and the substrate.

We have computed the formation energies of several O vacancies at the interface between the supported metallic Pt clusters decorated by CO molecules and the catalyst surface of the Pt_x/TiO_2 and Pt_x/Co_3O_4 (x = 1, 4, and 6) systems. The corresponding $FE(O_v)$ values are reported in Table 1. It is clear from Table 1 that, on the TiO_2 surface, the presence of supported Pt clusters lowers the values of $FE(O_v)$. Similar findings have been reported on Pt/Fe_3O_4,[49,68] Cu/TiO_2,[69] and Au/TiO_2[70] systems, where the presence of supported metal clusters has shown to facilitate the formation of O vacancies.

https://doi.org/10.1021/acs.jpcc.3c05714
J. Phys. Chem. C 2023, 127, 21132−21149

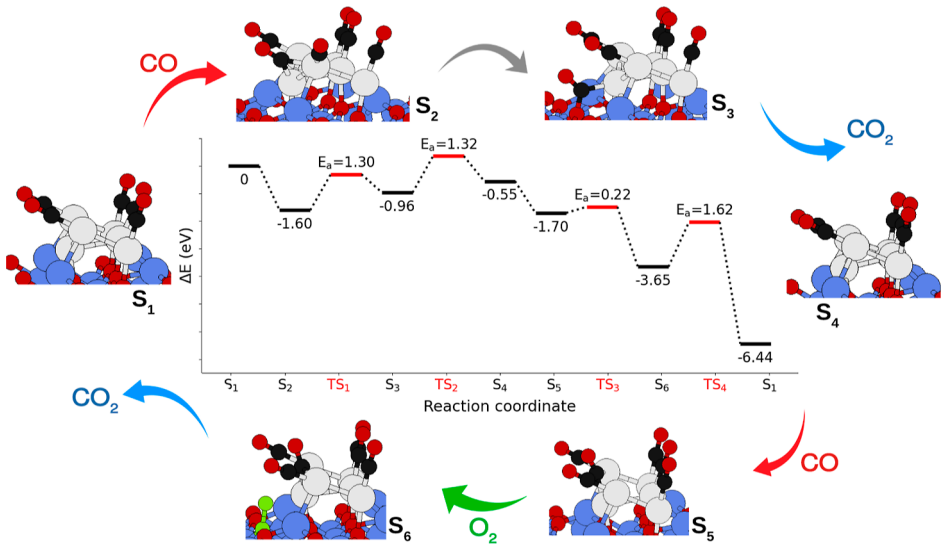

Figure 9. Energy profile of the MvK mechanism for CO oxidation on the Pt_6 cluster supported on Co_3O_4.

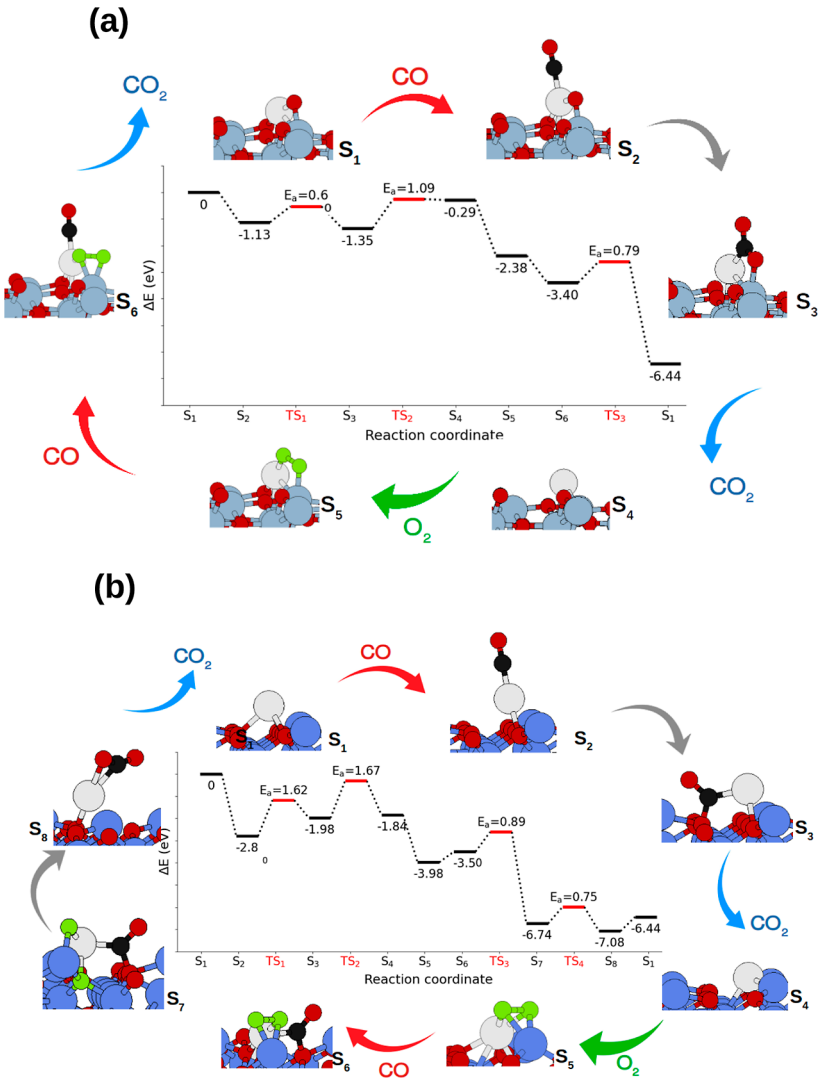

Figure 10. Catalytic cycle and energy diagram of CO oxidation on a) Pt_1-adatom/TiO_2 and (b)Pt_1-adatom/Co_3O_4 catalysts.

On the other hand, we found that on the Co_3O_4 surface the FE(O_v) are not influenced by the presence of supported Pt clusters except for the Pt_1/Co_3O_4 system. We note, however, that larger Pt NPs (>2 nm) supported on Co_3O_4 have been

https://doi.org/10.1021/acs.jpcc.3c05714
J. Phys. Chem. C 2023, 127, 21132−21149

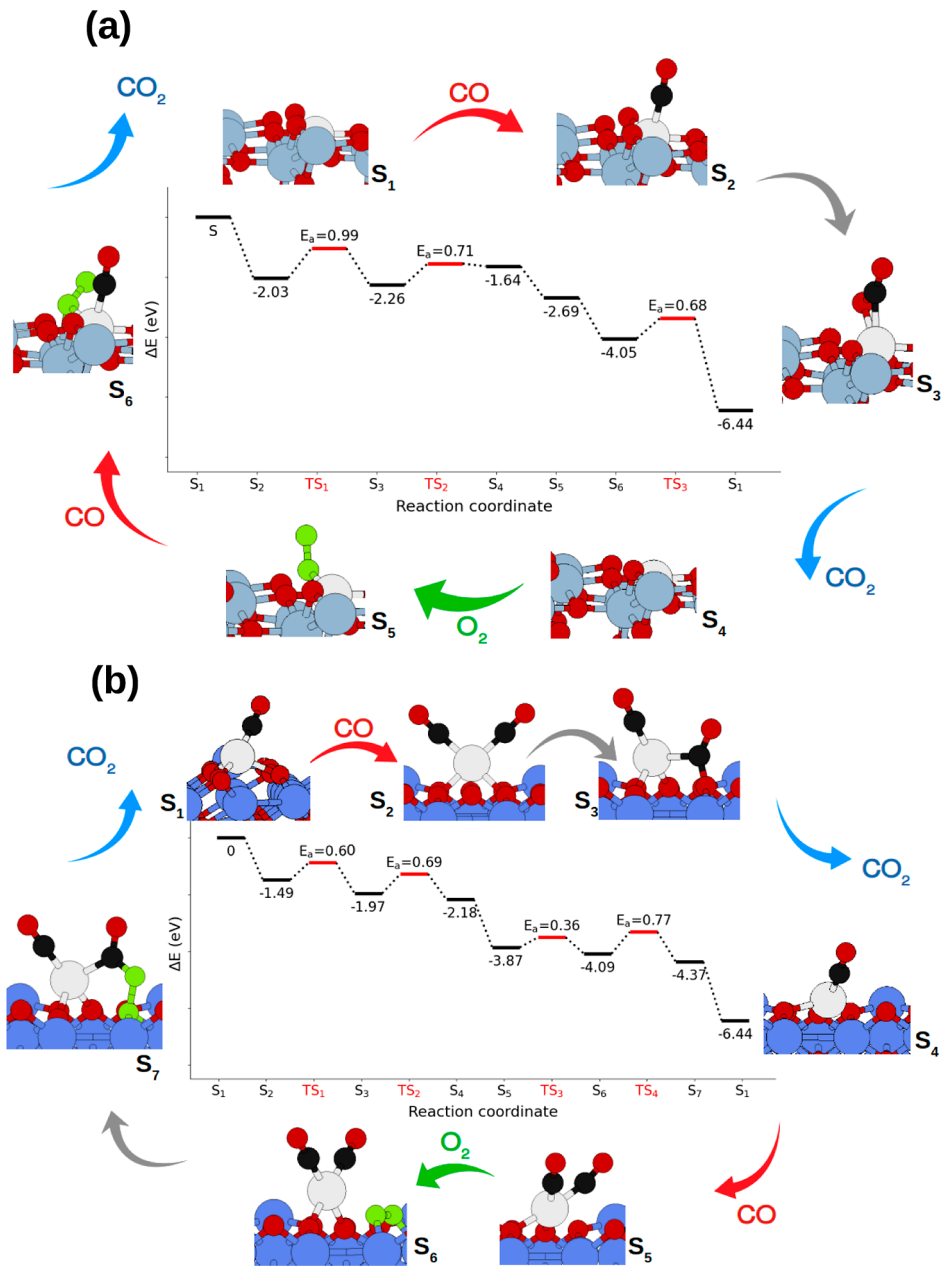

Figure 11. Catalytic cycle and energy diagram of the oxidation of CO on (a) $Pt_1(5c)/TiO_2$ and (b) $Pt_1(3c)/Co_3O_4$ systems.

shown to promote the formation of O_v and to induce strong metal−support interactions and formation of intermetallic compounds like Pt_3Co and CoO.[71]

The removal of an O atom from the stoichiometric TiO_2 surface gives rise to two excess electrons and the appearance of new electronic states in the band gap. The two excess electrons can be localized on any Ti atom, occupying Ti(3d) orbitals, thus formally creating Ti^{3+} sites. This also happens on the Pt_x/TiO_2 system, where the formation of an oxygen vacancy entails a strong charge rearrangement at the Pt/oxide interfaces. The spin density displayed in Figure 7 shows that the excess electrons resulting from the vacancy of the polarity of the ring mostly localize on two Ti sites.

We will now focus on the MvK reaction mechanism for CO oxidation on Pt_x/TiO_2 (x = 1, 4, and 6) and Pt_x/Co_3O_4 (x = 1 and 6) nanocatalysts that have been discussed in the previous sections. Additionally, we have investigated the CO oxidation on the TiO_2 and Co_3O_4 surfaces where Ti and Co atoms have been substituted with a Pt atom.

We can break down the MvK mechanism into several elementary steps. Starting with a Pt cluster with a free Pt site, in the first step, a gas-phase CO molecule is adsorbed on the cluster. A chemisorbed CO molecule then interacts with a lattice O atom leading to the formation of a chemisorbed CO_2 molecule. The desorption of CO_2 generates an O vacancy on the surface and a free Pt site. An O_2 molecule from the atmosphere then fills the vacancy, leading to an O_2 adsorbate bridging between the cluster edge and the support. A second CO molecule, adsorbed from the gas phase, interacts with an O atom of the newly adsorbed O_2 species forming a new CO_2 molecule, which will then desorb. The catalytic cycle is now closed, and the catalyst is back to the initial state.

Figure 8a,b shows a plot of the reaction path predicted by the NEB calculations for the CO oxidation on Pt_6 and Pt_4

https://doi.org/10.1021/acs.jpcc.3c05714
J. Phys. Chem. C 2023, 127, 21132−21149

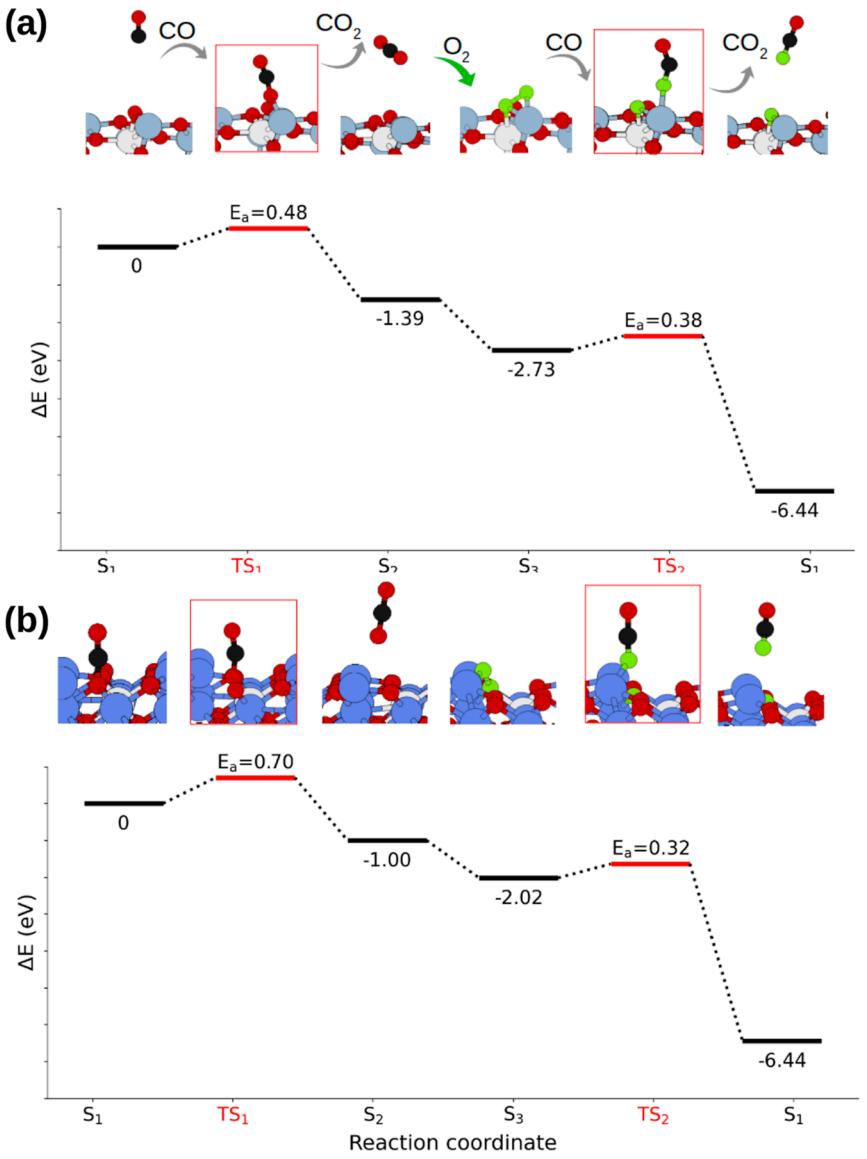

Figure 12. CO oxidation on oxides doped with $Pt_1(6c)$ on (a) TiO_2 and (b) Co_3O_4.

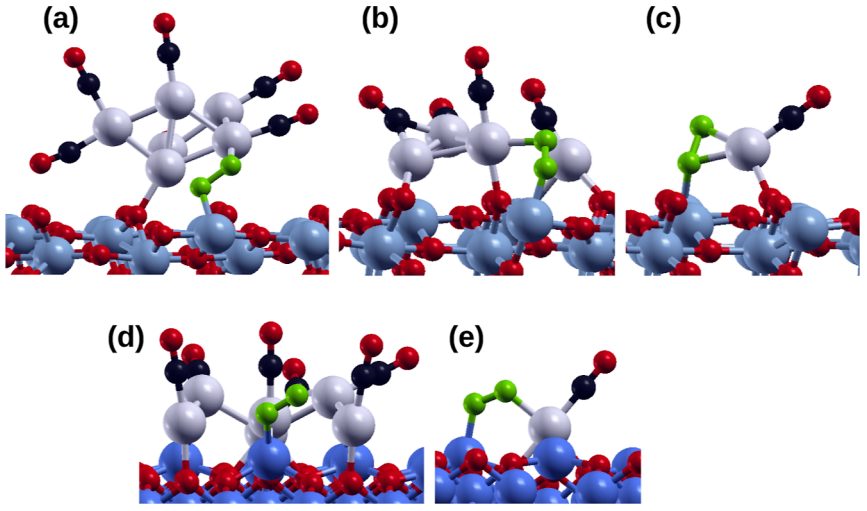

Figure 13. Molecular adsorption of O_2 at the interface of Pt_6, Pt_4, and Pt_1 on TiO_2 (a−c) and Pt_6 and Pt_1 on Co_3O_4 (d,e).

https://doi.org/10.1021/acs.jpcc.3c05714
J. Phys. Chem. C 2023, 127, 21132−21149

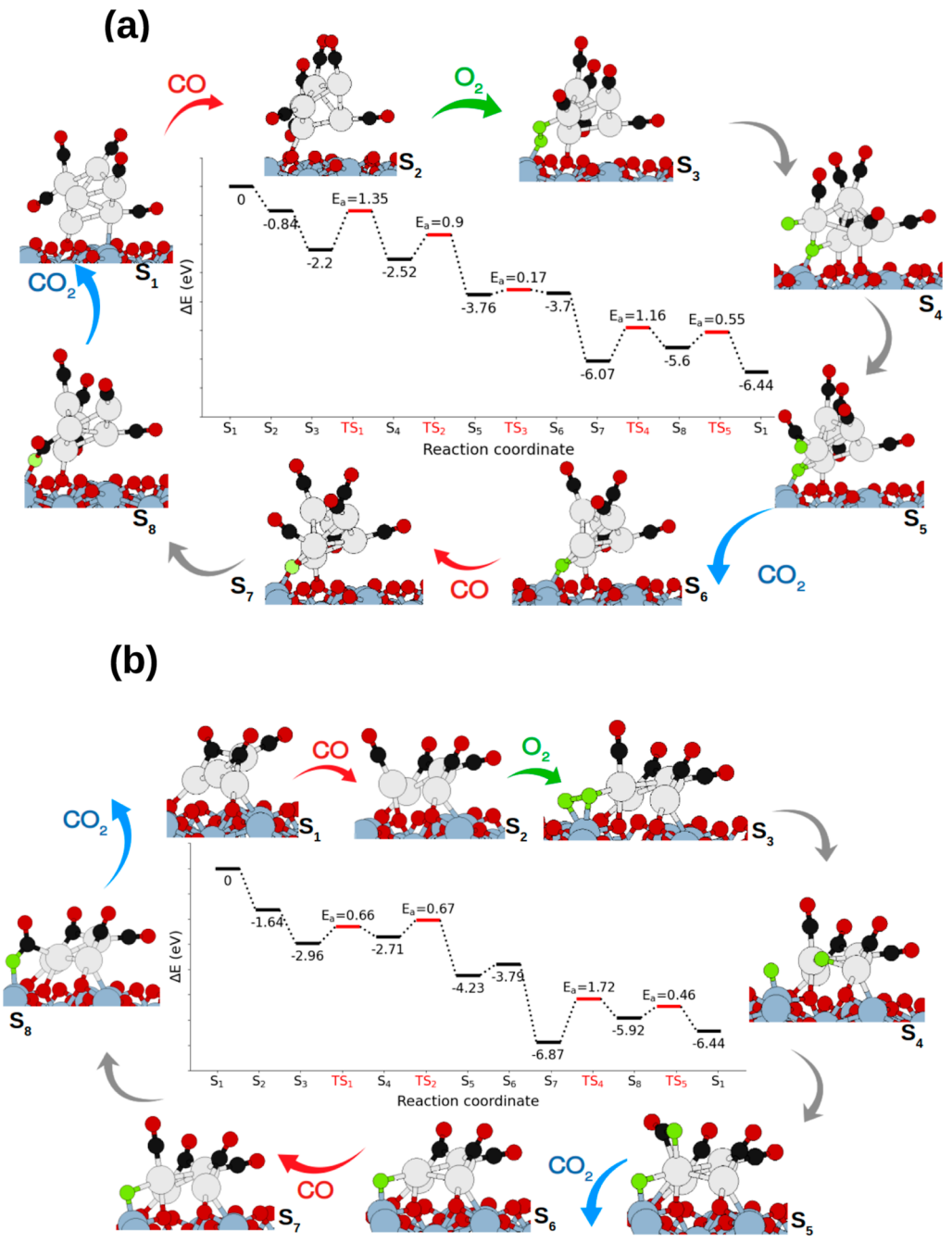

Figure 14. Steps of CO oxidation over (a) Pt_6 and (b) Pt_4 supported on TiO_2 via the LH mechanism.

clusters supported on the TiO_2 surface. In a full catalytic cycle, the reaction $2CO + O_2 \rightarrow 2CO_2$ takes place, while catalyst cycles among several intermediates, starting and ending with state S_1. The energies reported in Figure 8a,b are zero temperature energies, including those of reactants and products. The energy of the initial state, $S_1 + 2CO + O_2$, is set to zero, while the energy of the final state, $S_1 + 2CO_2$ is equal to the zero temperature reaction energy, −6.44 eV, to be compared against the experimental value of −5.70 eV. The same reaction mechanism has been investigated on the Pt_6/Co_3O_4 system, and it is depicted in Figure 9. We found that the energetics of the reaction is not favorable on Pt_4 supported on Co_3O_4. Hence, we skipped performing further simulations for Pt_4/Co_3O_4.

In the following, we will discuss all of the steps involved in the MvK catalytic cycle.

CO Adsorption. In the first step, a CO molecule binds on a vacant site on the supported Pt cluster already partially covered by CO molecules (Figures 8a,b and 9, $S_1 \rightarrow S_2$). Regardless of the type of support, the adsorption of CO on Pt clusters is exothermic and nonactivated. Full CO coverage on Pt_6/TiO_2 deforms the cluster drastically and weakens the interaction between the cluster and the support. This effect is less pronounced in the case of the Pt_6/Co_3O_4 system (see Figure 9, S_2), consistent with the stronger interaction of the metallic cluster with Co_3O_4 compared to TiO_2.

CO_2 Formation. The reaction proceeds through the oxidation of CO to CO_2 via a lattice oxygen atom, leading to the formation of an intermediate CO_2 species bound to the

https://doi.org/10.1021/acs.jpcc.3c05714
J. Phys. Chem. C 2023, 127, 21132−21149

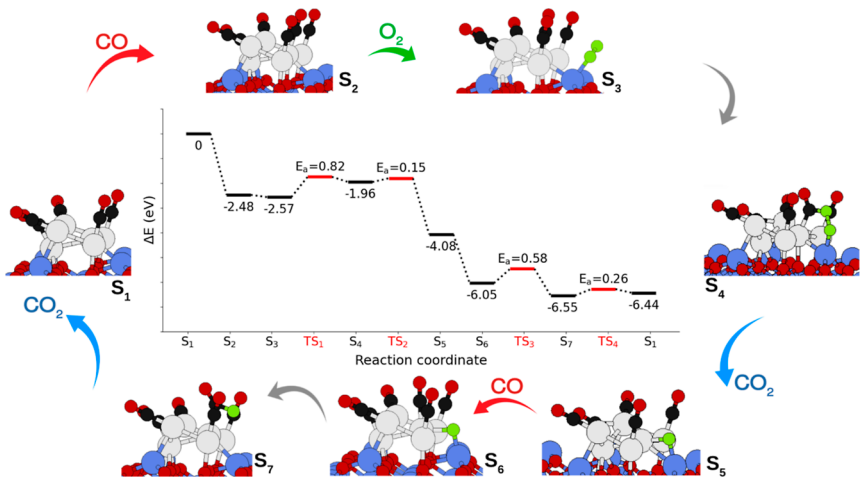

Figure 15. CO oxidation through the LH mechanism over Pt_6/Co_3O_4.

cluster, see Figure 8a,b, S_3. The formation of this intermediate represents the rate-limiting step of the overall reaction, requiring activation energies of 1.46/1.77 eV on the Pt_6/TiO_2 and Pt_4/TiO_2 systems, respectively. These values are decreased to 1.30 eV in the case of the Pt_6/Co_3O_4 system. This can be traced back to the values of formation energies of O vacancies on different supports: indeed, it is easier to remove an O atom from Pt_6/Co_3O_4 rather than on Pt_6/TiO_2, see Table 1. Similar activation energies (1.13 eV) have been reported for the Pt_4/CeO_2 system.[29] CO_2 formation via lattice oxygen is known to be an activated step in metal-/reducible oxide-supported catalysts.[13,59,70,72] Previous experimental work has shown that the oxidation of CO to CO_2 via O lattice atoms on a Au/TiO_2 catalyst occurs at high temperatures, around 120 °C, thus confirming that the reaction must overcome a significant energy barrier in order to occur.[13]

CO_2 Desorption. The last step of the first half-cycle of CO oxidation is the release of CO_2 from the catalysts. The activation energies associated with the desorption of CO_2 from the catalysts are found to be 0.31 and 0.64 eV, for Pt_6 and Pt_4 clusters supported on TiO_2 (see Figure 8, S_4), respectively. The corresponding value for the Pt_6/Co_3O_4 system (Figure 9, S_4) is 1.32 eV, meaning that the desorption of CO_2 is feasible on the Pt-supported TiO_2. In addition, the calculations suggest that the release of CO_2 from the catalyst to the gas phase ($S_3 \rightarrow S_4$) is slightly exothermic on the Pt_6/TiO_2 system, but it costs almost 0.5 eV on Pt_4/TiO_2 and Pt_6/Co_3O_4 nanocatalysts. The oxidation of CO and desorption of CO_2 via an O lattice atom generate an O vacancy on the surfaces and result in a significant structural rearrangement of the metallic cluster.

O_2 Adsorption and Catalyst Regeneration. The support can be reoxidized in the presence of gas-phase molecular O_2. There is indeed a strong driving force for the binding of molecular O_2 on the surface O vacancy. However, on the Pt_4/TiO_2 system, the O vacancy left behind after the desorption of CO_2 is located underneath the Pt cluster and thus is not accessible to O_2. Therefore, we propose an alternative path where a lattice O atom diffuses into the O vacancy, filling it, and forming a new O vacancy that is now exposed to molecular O_2. The activation energy associated with the diffusion of the O vacancy is found to be 1.49 eV (Figure 8b), $S_5 \rightarrow S_6$). There is a strong driving force for the binding of O_2 to the O vacancy for all of the systems investigated. The process is barrierless on the Pt_4/TiO_2 and Pt_6/TiO_2 nanocatalysts, whereas a small energy barrier (E_a = 0.22 eV, Figure 9, $S_5 \rightarrow S_6$) must be overcome on the Pt_6/Co_3O_4 system. The next step is dissociation of the newly adsorbed O_2 molecule. Our calculations suggest that this step is once again barrierless on Pt_4/TiO_2 and Pt_6/Co_3O_4, while on Pt_6/TiO_2 there is an activation energy of 0.13 eV (Figure 8. S_7).

These results are in line with a recent combined experimental and theoretical work focusing on an Au/TiO_2 system, where the catalyst was reduced at the end of the first half of the cycle, and then it was reoxidized by O_2 pulses at different temperatures (−20 to +240 °C). It was observed that O_2 consumption by the catalyst did not change remarkably as the temperature increased.[70] The same work, on the basis of DFT calculations, predicts that filling O vacancies is barrierless because of the coexistence of adjacent vacancies in the lattice, and in the case of a single oxygen vacancy this step is activated by a small barrier of 0.16 eV. In contrast, a relatively high energy barrier (0.41 eV) was predicted for O_2 dissociation on $Pd/CeO_2(100)$, whereas on Fe_2O_3-supported Pt NPs, O_2 dissociation turned out to be the rate-determining step of CO oxidation through the MvK mechanism.[49]

Formation and Desorption of a Second CO_2 Molecule. After adsorption and dissociation of molecular O_2 at the vacancy sites, the system stoichiometry is restored and an extra O atom adsorbed as an adatom is present on the surface. This excess of the O atom may react with CO adsorbed on the supported Pt metallic cluster to form a CO_2 molecule or fill an additional surface O vacancy if present. However, the calculations suggest that the cost to create a new O vacancy on the Pt_6/TiO_2 surface in the proximity of the excess O adatom is 2.95 eV, which is therefore thermodynamically highly unfavorable. Hence, we focused on the oxidation of a second CO_2 molecule via the excess of the O atom on the surface. On Pt_6/TiO_2 and Pt_4/TiO_2, the activation energies for the formation of this second CO_2 molecule are 0.87 and 0.75 eV, respectively (see Figure 8a,b, S_8), whereas the desorption of the newly formed CO_2 molecule has a barrier lower than 1 eV on both systems (S_9). Instead, on Pt_6/Co_3O_4, the formation and desorption of a second CO_2 molecule occurs in a single step (Figure 9, $S_6 \rightarrow S_7$) with an activation energy of 1.62 eV.

Comparing the results for the MvK mechanism on the systems examined so far, looking at the elementary step with the highest activation energy, we find that in the case of both Pt_6/TiO_2 and Pt_4/TiO_2, the slowest step is the formation of

https://doi.org/10.1021/acs.jpcc.3c05714
J. Phys. Chem. C 2023, 127, 21132−21149

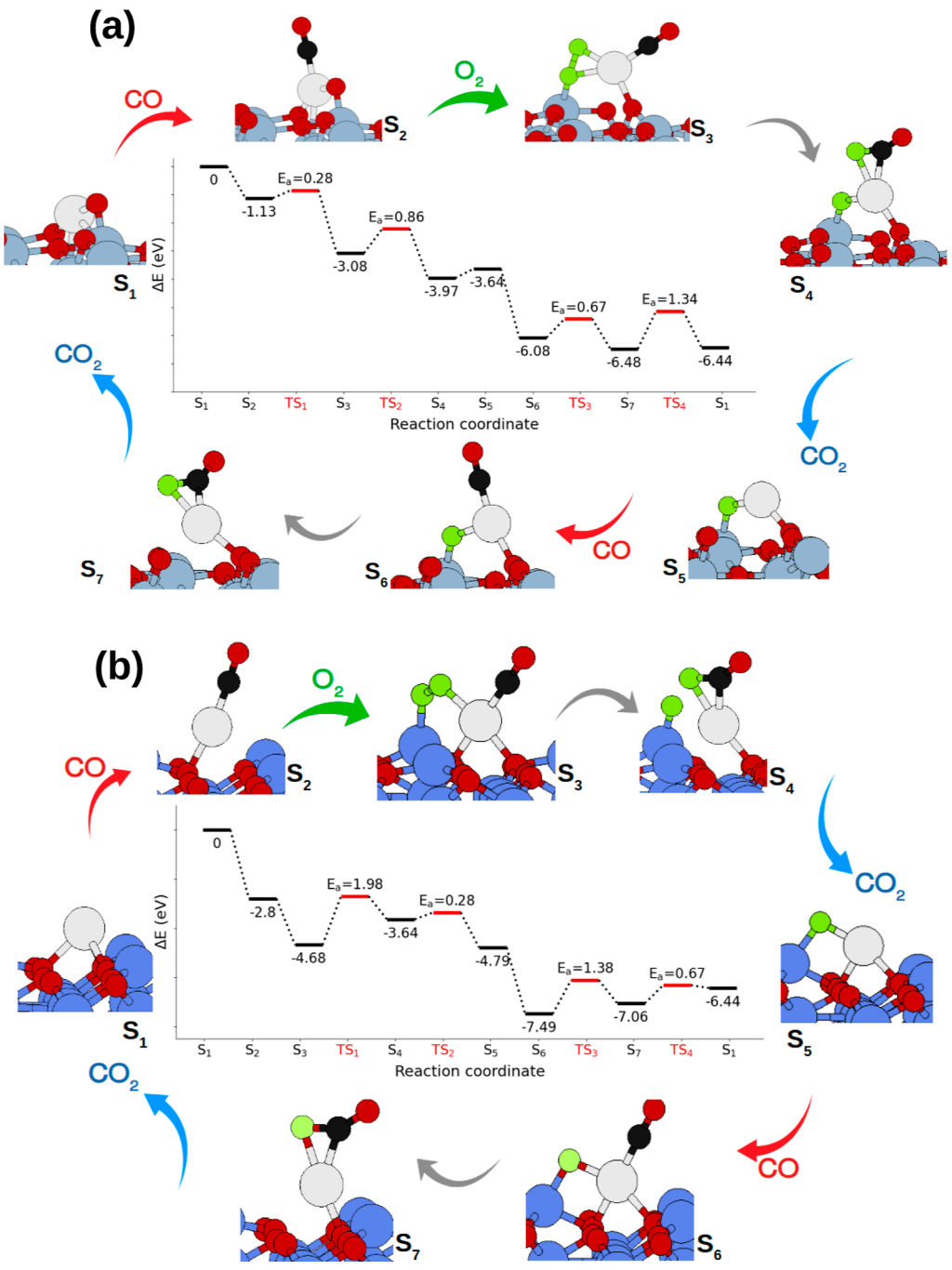

Figure 16. LH mechanism for CO oxidation on a Pt_1-adatom supported on the surface of (a) TiO_2 and (b) Co_3O_4.

the first CO_2 molecule involving the creation of a vacancy in the support; in the case of Pt_6/Co_3O_4, on the other hand, the step with the largest barrier is the formation of and desorption of the second CO_2 molecule.

MvK Mechanisms on Single-Atom Pt Catalysts. Next, we considered the reaction mechanism for CO oxidation in the case of a single Pt atom adsorbed as an adatom or as a substitutional ion on the TiO_2 and Co_3O_4 substrates. In the substitutional case, on both supports, two different possibilities have been considered: on the TiO_2 support, we have substituted a Ti ion coordinated with five or six lattice oxygen atoms with a Pt ion (denoted $Pt_1(5c)$ and $Pt_1(6c)$, respectively), whereas on the Co_3O_4 substrate, we have replaced a Co^{2+} or Co^{3+} ion with Pt, resulting in a three-coordinated ($Pt_1(3c)$) or six-coordinated ($Pt_1(6c)$) Pt ion. We will first examine $Pt_1(5c)$ on TiO_2 and $Pt_1(3c)$ on Co_3O_4, since in both cases the substitutional atom is not fully coordinated to an octahedron of the O atoms. Next, we will consider $Pt_1(6c)$ on both supports, since in this case the substitutional atom does not have any missing ligand where the adsorption of CO and/or O_2 might take place.

MvK Mechanisms on the Pt_1-Adatom. In its most stable configuration, a Pt_1-adatom binds to two oxygen atoms-on TiO_2, one of which is 2-fold-coordinated to Ti atoms and the other one 3-fold-coordinated, with an adsorption energy of 2.27 eV. The 2-fold-coordinated oxygen was dislodged by Pt adsorption (Figure 10a, S_1); this oxygen with $FE_{O_v} \sim 0.9$ eV is the easiest one to remove around the Pt-adatom.

https://doi.org/10.1021/acs.jpcc.3c05714
J. Phys. Chem. C 2023, 127, 21132−21149

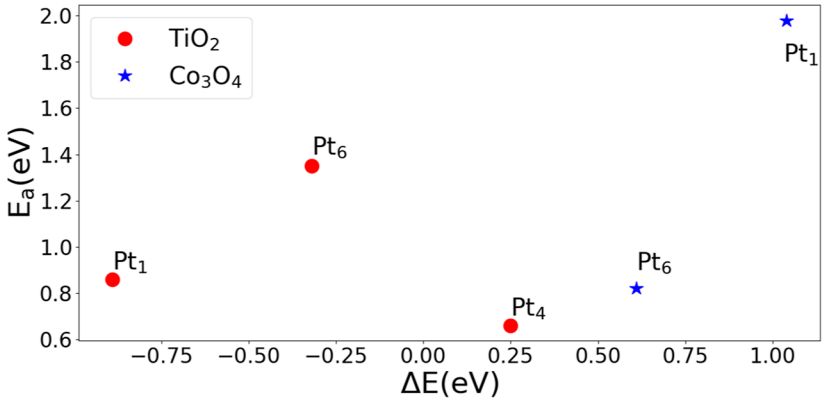

Figure 17. Calculated activation energies (E_a) and reaction energy (ΔE) for the dissociation of chemisorbed O_2 on Pt catalysts supported on TiO_2 and Co_3O_4.

Table 2. Activation Energy of the Most Demanding Elementary Step along the Catalytic Cycle of CO Oxidation on Each System Investigated for Both the LH and MvK Reaction Mechanisms[a]

system	E_a for MvK (eV)	E_a for LH (eV)	predicted mechanism
Pt_6/TiO_2	1.46	1.35	LH
Pt_4/TiO_2	1.77	1.72	LH
Pt_1/TiO_2	1.09	1.34	MvK
$Pt_1(5c)/TiO_2$	0.99		MvK
$Pt_1(6c)/TiO_2$	0.48		MvK
Pt_6/Co_3O_4	1.62	0.82	LH
Pt_1/Co_3O_4	1.67	1.98	MvK
$Pt_1(5c)/Co_3O_4$	0.77		MvK
$Pt_1(6c)/Co_3O_4$	0.70		MvK

[a] Pt_6, Pt_4, and Pt_1 are supported clusters, while $Pt_1(5c)$ and $Pt_1(6c)$ are Pt atoms replacing a surface Ti or Co surface ion, either 5-fold- or 6-fold-coordinated.

The formation of the first CO_2 molecule (S_3 in Figure 10e, MvK single adatom) is slightly exothermic (−0.22 eV) on TiO_2 with a barrier of 0.60 eV, while on Co_3O_4 it is endothermic by 0.82 eV and has an activation energy of 1.62 eV. The desorption of CO_2 (S_4) exhibits the highest E_a in the catalytic cycle on both types of supports: 1.09 and 1.67 eV on TiO_2 and Co_3O_4, respectively. After the removal of the first CO_2, the Pt-adatom was bonded to two metal atoms in the case of TiO_2 and to three atoms in the case of Co_3O_4.

For the following step, we considered both the possibility of O_2 and CO adsorption. We found that the adsorption energy of O_2 is −2.09 eV, while the adsorption energy of CO is −1.98 eV. We therefore assume that the adsorption of O_2 as our next step would be more probable ($S_4 \rightarrow S_5$), followed by the adsorption of the CO ($S_5 \rightarrow S_6$).

The formation and desorption of the second CO_2 via the activation of chemisorbed O_2 occurs in a single step on TiO_2 (Figure 10a, $S_6 \rightarrow S_7$). In the case of Co_3O_4, O_2 first dissociates, and one of the O atoms fills the O vacancy created during the oxidation of the first CO molecule, with an activation energy of 0.89 eV (Figure 10b, $S_6 \rightarrow S_7$). The leftover O atom then oxidiz the CO molecule with a barrier of 0.75 eV ($S_7 \rightarrow S_8$), followed by CO_2 desorption, an activated step with a barrier of 0.65 eV.

Comparing now the results for the MvK mechanism on the Pt_1-adatom on the two supports, we found that in both cases the most activated elementary step is the desorption of the first CO_2 molecule, with barriers of 1.09 and 1.67 eV for TiO_2 and Co_3O_4, respectively. Comparing these quantities to the most demanding step for the larger clusters examined earlier, we found that Pt_1 seems to improve the kinetics of the CO oxidation of TiO_2 but not of Co_3O_4.

Comparing our results for Pt_1 on brookite TiO_2 with those of Bac and Mallikarjun Sharada[73] on TiO_2 rutile, we found very large differences. In particular, the most demanding step for the formation of CO_2 via MvK on rutile was predicted to have an enormous barrier of 5.39 eV. This suggests that different polymorphs can have vastly different kinetics for the MvK mechanism.

MvK Mechanisms on Not Fully Coordinated Substitutional Pt_1. Next, we considered the case in which Pt_1 substitutes a surface cation atom of the support. In this section we focus on cation surface sites that are not fully coordinated with an octahedron of six O atoms, while the 6-fold-coordinated sites will be discussed in the following section.

Similar to the MvK mechanism on TiO_2-supported Pt clusters, the most demanding step on $Pt_1(5c)/TiO_2$ was predicted to be the formation of CO_2 with lattice oxygen. This step has a barrier of 0.99 eV (Figure 11a, $S_2 \rightarrow S_3$), which is close to the quantity found for the Pt_1-adatom (1.09 eV). Moreover, similar to the case of the Pt_1-adatom, the formation and desorption of the second CO_2 on $Pt_1(5c)/TiO_2$ happen in a single step with an E_a of 0.68 eV. Also, for this step, the activation energy is comparable to the barrier for the same step on the Pt_1-adatom (0.79 eV).

Moving now to the case of Co_3O_4, we examined the case of Pt_1 substituting a 3-fold-coordinated Co (see Figure 11b). At variance with the Pt_1/TiO_2 system, in this case, we found that it is possible to coadsorb two CO molecules on a Pt atom, and this structure is slightly more favorable than the system with one CO. One of the CO molecules reacts with lattice oxygen, and the formation and desorption of CO_2 have similar energy barriers (0.60 and 0.69 eV, respectively). In the next step ($S_4 \rightarrow S_5$), a CO molecule is adsorbed, followed by the adsorption of molecular oxygen to fill the lattice vacancy. The adsorption of oxygen is an activated step with an activation energy of 0.36 eV. The formation of the second CO_2 molecule has the highest barrier in the cycle (0.77 eV, $S_6 \rightarrow S_7$). The desorption of the second CO_2 is not activated and is highly exothermic.

It is interesting to compare our findings with calculations performed on Pt_1 substituting a Ce^{4+} ion in CeO_2. The energy

https://doi.org/10.1021/acs.jpcc.3c05714
J. Phys. Chem. C 2023, 127, 21132−21149

barrier to form and desorb CO_2 on $Pt_1/CeO_2(110)$ was predicted to be 1.31 eV if the reaction goes through the MvK mechanism.[74] On the same support but exposing the (111) termination, the predicted activation energy was much higher (2.38 eV).[75]

MvK Mechanism on Fully Coordinated Substitutional Pt_1.[76,77] By replacing a fully coordinated metallic atom of the support surface with a single Pt, CO oxidation proceeds via indirect assistance of Pt, as depicted in Figure 12a,b.

The dissociative reaction between CO and lattice oxygen over $Pt_1(6c)$ occurs according to similar steps on both types of oxides. CO(g) reacts with the oxygen atom, which is bonded on top of $Pt_1(6c)$. To remove this oxygen, 1.83 eV of energy is required on TiO_2. On Co_3O_4, however, $E_{form_{O_v}}$ associated with this oxygen is 2.22 eV, which is more than $E_{form_{O_v}}$ on pristine Co_3O_4. A recent study on the interaction between the Pt atom and rutile (110) revealed that substituting a six-coordinated Ti with Pt makes the formation of oxygen vacancies easier and stabilizes the oxygen vacancies against migration.[78] In the case of Pt_1 on CeO_2, removal of lattice oxygen was 1 eV more endothermic in the presence of a single Pt-adatom compared to bare CeO_2. However, doping CeO_2 with atomic Pt made it easy to remove the oxygen in the vicinity of Pt.[74]

Local optimization of the catalyst with a CO molecule adsorbed on lattice oxygen (*CO) leads to the simultaneous formation and desorption of CO_2. Adsorption of CO(g) and formation and desorption of CO_2 take place in one step, with the formation of $*CO_2$ being the transition state. The activation energy corresponding to this step is higher on Co_3O_4 (0.70 eV) than on TiO_2 (0.48 eV).

Sequential adsorption of O_2 and filling of the lattice vacancy are nonactivated and exothermic by more than −2 eV. After filling the oxygen vacancy, one atomic oxygen is chemisorbed on the surface which readily reacts with another CO(g) to form CO_2. Formation and desorption of the second CO_2 are associated with moderate energy barriers on both supports: 0.38 and 0.32 eV on TiO_2 and Co_3O_4, respectively.

As one can see, the catalytic performance of Pt_1 is different on two different types of supports in this work. In an experimental study, SACs were synthesized on highly reducible Fe_2O_3, reducible ZnO, and irreducible Al_2O_3. It was found that the reaction rate on a single-atom Pt is related to the reducibility of the supporting surface.[79] However, in the present work, except for $Pt_1(3c)$, the rest of the Pt catalysts show lower activation energy on the less reducible surface.

In an experimental investigation on Pt_1/rutile with Pt substituting a Ti atom, the highest barrier associated with CO conversion was found to be 22.7 kJ/mol^{-1} (~0.2 eV), which was in line with the computed barrier from DFT simulation of the same system (19 kJ/mol^{-1});[80] these results are numerically comparable with our findings.

In a theoretical work on Pt_1/CeO_2, the stable structure was detected to be Pt substituting a six-coordinated Ce atom; two CO molecules formed CO_2 with lattice oxygen atoms sequentially, and then two vacancies were filled via dissociative adsorption of one molecular oxygen, which was found to be the rate-determining step of the cycle.[77] Pt atoms doped into the CeO_2 surface were found to be highly active for CO oxidation catalysis.[75]

LH Mechanism on Pt_x Clusters. In analogy to the MvK mechanism, the oxidation reaction was modeled on Pt_6 and Pt_4 clusters supported on TiO_2 as well as Pt_6 supported on Co_3O_4. We also considered the cases of single Pt atom catalysts, both as adatoms and substitutional ions.

Since the adsorption of CO on the Pt_6/TiO_2 cluster is much more favorable (E_{ads}^{CO} = −2.30 eV) than the adsorption of molecular oxygen ($E_{ads}^{O_2}$ = −1.35 eV), at similar partial pressures of gas-phase species, the cluster will be mostly covered by CO. A similar scenario was predicted on Pt_4/TiO_2, on which E_{ads}^{CO} and $E_{ads}^{O_2}$ were found to be −2.29 and −1.53 eV, respectively. We therefore examined the adsorption of O_2 on the Pt systems, which are already fully covered by CO.

Figures 14a,b and 15 display the energetics and structure of the intermediates for CO oxidation on Pt clusters supported on TiO_2 and Co_3O_4 via the LH mechanism. In the following, we briefly describe the sequence of elementary steps.

CO Adsorption on the Pt Cluster. Assuming as the starting point of the catalytic cycle a system where there is a single vacant site for CO adsorption, the first step of the cycle is the nonactivated adsorption of a CO molecule to reach full coverage (1 CO per Pt).

O_2 Adsorption. The most favorable site for adsorption is at the interface between the Pt cluster and the support, as shown in Figure 13a−c, with adsorption energies of −1.37, −1.42, and −1.95 eV per molecule on Pt_6, Pt_4, and Pt_1/TiO_2, respectively. On Co_3O_4, however, the Pt_6 cluster is bound significantly more strongly than in the case of TiO_2.[44] This leads to a structure where the Pt atoms are more coordinated compared to Pt_6 on TiO_2, and the incoming O_2 binds to a surface Co atom rather than to Pt, with a weak adsorption energy of −0.09 eV. In the case of Pt_1 on Co_3O_4, O_2 binds very strongly, with an adsorption energy of −1.88 eV (Figure 13d,e). Similar to CO adsorption, adsorption of O_2 is nonactivated (step S_3 in Figure 14a,b and in Figure 15).

O_2 Dissociation. On TiO_2-supported clusters, the dissociation of O_2 is an activated step, with energy barriers of 1.35 eV on Pt_6 and 0.66 eV on Pt_4 (Figure 14a,b, $S_3 \rightarrow S_4$). O_2 dissociation was found to be the limiting step of the oxidation reaction through the LH mechanism on Pt particles (1.8−25 nm).[81] The dissociation of O_2 on Pt_6 exhibits the highest energy barrier in the cycle. In the case of Pt_6/Co_3O_4, on the other hand, O_2 activation takes place via the formation of a new intermediate, where one of the O atoms of O_2 binds to the C atom of a chemisorbed CO molecule (Figure 15, S_4). The formation of this CO−O_2 intermediate is endothermic and has a barrier of 0.82 eV. This is the highest energy barrier for the whole cycle on Pt_6/Co_3O_4. The cleavage of the O−O bond and the formation of the CO_2 molecule take place in a concerted manner Figure 14, $S_4 \rightarrow S_5$), as discussed below.

Formation of CO_2. After the dissociation of O_2, a CO molecule diffuses toward the atomic oxygen to form CO_2 ($S_4 \rightarrow S_5$ in Figure 14a,b and S_4 in Figure 15). This step has activation energies of 0.90 and 0.67 eV on Pt_6 and Pt_4 on TiO_2, respectively. In the case of Pt_6/Co_3O_4, the formation of CO_2 from the CO−O_2 intermediate is strongly exothermic and weakly activated, with a barrier of just 0.15 eV. At the end of this step, the newly formed CO_2 molecule is not bound to the cluster and desorbs to the gas phase (S_5 in Figure 15).

Desorption of CO_2. CO_2 is weakly adsorbed on both Pt_6/TiO_2 (0.06 eV) and Pt_4/TiO_2 (0.44 eV). After this step, the catalysts have an excess of one O atom compared to the initial state.

CO Adsorption. As in the case of the adsorption of the first CO molecule, CO adsorption is nonactivated and largely

https://doi.org/10.1021/acs.jpcc.3c05714
J. Phys. Chem. C 2023, 127, 21132−21149

exothermic, with an adsorption energy exceeding 2 eV in all three systems.

Formation of Second CO_2. The next step is the formation of a second CO_2 molecule with an excess O atom ($S_7 \rightarrow S_8$ on TiO_2 and $S_6 \rightarrow S_7$ on Co_3O_4). While the formation of the second CO_2 has a moderate E_a (0.58 eV) on Pt_6/Co_3O_4, the barrier is 1.16 and 1.72 eV on Pt_6/TiO_2 and Pt_4/TiO_2, respectively, which makes this step the most demanding step of CO oxidation on Pt_4/TiO_2.

Desorption of the Second CO_2 Molecule. This last step is just slightly more difficult than desorption of the first CO_2 on Co_3O_4. However, the removal of the second CO_2 on TiO_2 is activated, with the barrier of 0.55 and 0.46 eV on Pt_6 and on Pt_4, respectively. This step closes the catalytic cycle and regenerates the initial state of the catalyst.

LH Mechanism on the Pt_1-Adatom. The computed oxidation path and the energy profile of the oxidation reaction on a Pt_1 adatom on both supports are displayed in Figure 16a,b. The initial step of the catalytic cycle is the adsorption of CO ($S_1 \rightarrow S_2$) which is much more exothermic on Co_3O_4 (−2.80 eV) compared to that on TiO_2 (−1.13 eV). The adsorption of O_2 ($S_2 \rightarrow S_3$) is slightly activated (E_a = 0.28 eV) on TiO_2 and nonactivated on Co_3O_4, and in both cases it is strongly exothermic (−1.95 eV on TiO_2 and −1.88 eV on Co_3O_4). On TiO_2, in the final structure after adsorption of both CO and O_2 (state S_3), Pt is uplifted and bound to a single surface O atom, while on Co_3O_4 the position of Pt is only weakly perturbed compared to the initial structure.

Searching for the minimum energy path between state S_3 and a chemisorbed CO_2 molecule (state S_4), we found that the dissociation of the O−O bond and the formation of the O−C bond of the CO_2 molecule take place simultaneously. This step on TiO_2 is exothermic (−0.89 eV) and has a barrier of 0.86 eV. For the same reaction step on Pt_1/TiO_2 (rutile), E_a was predicted to be 0.90 eV,[73] very close to what we predicted on brookite. On Co_3O_4, it is highly endothermic (1.04 eV) and has a large activation energy (1.98 eV).

The desorption of CO_2 ($S_4 \rightarrow S_5$) is endothermic on TiO_2 (0.33 eV) and exothermic on Co_3O_4 (−1.15 eV) with a barrier of 0.28 eV.

Adsorbing another CO molecule on the catalyst is highly favorable on both supports (−2.44 eV on TiO_2 and −2.70 eV on Co_3O_4). The formation of the second CO_2 ($S_6 \rightarrow S_7$) has activation energies of 0.67 on TiO_2 and 1.38 eV on Co_3O_4. To remove the second CO_2 molecule and close the cycle, a substantial barrier of 1.34 eV should be overcome on TiO_2, a value twice as large as the barrier on Co_3O_4, 0.67 eV.

Considering our simulations on Pt_1 adsorbed on TiO_2 and Co_3O_4, one can see that the highest energy barrier on TiO_2 is 1.34 eV, corresponding to the removal of the second CO_2, whereas the most activated step on Co_3O_4 is the breaking of the O−O bond and the concomitant formation of CO_2, which has an activation energy of ∼2 eV.

A non-MvK oxidation path was reported on Pt_1 supported on nonreducible Al_2O_3.[82,83] However, in the present work, the MvK mechanism is predicted to be an easier reaction channel than LH on Pt_1 if supported on reducible metal oxides like TiO_2 and Co_3O_4. Another ab initio study on irreducible Al_2O_3 predicted a LH-like mechanism for CO oxidation on Pt_1: adsorption of O_2 was more favorable than that of CO, and hence adsorption of CO on oxidized Pt_1 led to the formation of a carbonate ($-CO_3$) intermediate. The activation of the carbonate to release CO was found to be highly endothermic, and unless the reaction is run at high temperatures, the catalyst is predicted to be covered by carbonate.[82] A comparison of these studies indicates the crucial role of the type of supporting oxide in the CO oxidation mechanism on Pt_1 adatoms. Our findings are in agreement with a DFT study of reducible $Pt_1/CeO_2(110)$: the highest activation energy for the MvK mechanism was predicted to be 1.31 eV, while it increased to 2.15 eV when the reaction proceeded via the LH mechanism.[74]

Comparing the highest activation barriers for the LH mechanism on Pt_x systems with different sizes, we notice that on TiO_2, Pt_6 and Pt_1 would perform similarly. However, Pt_4 shows a higher E_a value than Pt_6 via the LH mechanism. In agreement with our findings, Pt_1/FeO_x had a higher rate for CO oxidation via the LH mechanism compared to Pt clusters and Pt NPs.[33] Also, experimental investigation on Pt catalysts adsorbed on anatase demonstrated that Pt_1 is at least 4 times more active than Pt clusters (∼1 nm) in the oxidation of CO.[30]

On the other hand, considering now the Pt_x/Co_3O_4 catalysts, CO oxidation on occurs on the Pt_6 cluster with a mild value of activation energy (0.82 eV), whereas Pt_1 does not seem to be an efficient catalyst for CO oxidation. This is vividly additional evidence that the catalytic behavior of Pt clusters is strongly affected by both the type of support and the catalyst size.

Further, we tried to complete our study by finding a descriptor in order to explain the different behaviors of the Pt catalysts. It was reported[28] that there is a correlation between the number of edge Pt atoms and the number of produced CO_2 molecules through the MvK mechanism. In the present work, however, considering the small size and 3D structure of Pt systems and also the fluxionality of the clusters, we cannot claim the same.

Another possibility is to find a linear correlation between the activation energy and the reaction energy of some of the elementary steps along the catalytic cycle, known as the Brønsted−Evans−Polanyi relation.[84] Here, as an elementary step, we considered the dissociation of chemisorbed O_2. As depicted in Figure 17, neither a linear relationship between the activation energy and the reaction energy nor a size-dependent trend was found.

To summarize our findings schematically, we show in Table 2, for each of the systems investigated, the activation energy of the most demanding elementary step along the catalytic cycle of CO oxidation for both the LH and MvK mechanisms. Assuming the active mechanism is the one with the smallest barrier for the most demanding step, the last column reports which mechanism should be active.

Conclusions. Numerous efforts have been dedicated to investigating the catalytic properties of Pt NPs in different applications. Yet, subnanometer Pt catalysts are relatively underexamined. We conducted a thorough study of the catalytic activity of metallic and oxidized Pt clusters as well as single-atom Pt supported on TiO_2 and Co_3O_4 toward the oxidation of CO to CO_2. Our DFT modeling confirms that the Pt/metal oxide interfaces provide active sites for the reaction between oxygen and CO molecules. Moreover, our simulations show that for Pt catalysts supported on reducible surfaces, such as TiO_2 and Co_3O_4, conversion of CO into CO_2 can involve oxygen atoms from the lattice. We found an enhancement in the reducibility of TiO_2 after the adsorption of Pt. We modeled the reaction paths of both MvK and LH mechanisms on Pt_6, Pt_4, and Pt_1. On TiO_2, while a small cluster such as Pt_4 showed

https://doi.org/10.1021/acs.jpcc.3c05714
J. Phys. Chem. C 2023, 127, 21132−21149

relatively high activation energy for both MvK and LH, a larger cluster like Pt_6 was found to have lower barriers, and Pt_1 demonstrated the best performance, possessing the lowest barriers. This is the opposite of what was predicted on Co_3O_4, where Pt_1 performs poorer than Pt_6, regardless of the type of the mechanism. One can note the significant role of the cluster size and the type of reducible supports in the catalytic performance of Pt nanoclusters. Further, the slowest step in the MvK oxidation mechanism on TiO_2 was found to be extracting lattice oxygen, whereas removing the product is the rate-limiting step on Co_3O_4. We point out that there is no correlation between the cost of creating the oxygen vacancy and kinetics of CO oxidation on Pt nanocatalysts, as a lower FE_{O_v} on Co_3O_4 did not facilitate the MvK mechanism on this oxide. On the other hand, substituting a metal atom of the surface by a single Pt assisted the extraction of lattice oxygen for both oxides, and hence lower activation energies were predicted for MvK on doped surfaces.

For the LH mechanism, we found the dissociation of oxygen to be rate-determining only on Pt_6/TiO_2. Similar to the case for MvK, the removal of CO_2 was predicted to be the slowest step of the cycle for other systems.

Our simulations suggest that Pt clusters are active catalysts when they are supported on Co_3O_4. In addition, in spite of many theoretical and experimental works proving the remarkable performance of the Pt_1 catalyst on different supports, our findings predict that this is probably not the case on Co_3O_4. The single-atom Pt catalyst was active only when an atom was substituted from the Co_3O_4 lattice.

AUTHOR INFORMATION

Corresponding Author

Simone Piccinin − *CNR-IOM, Consiglio Nazionale delle Ricerche, Istituto Officina dei Materiali, Trieste 34136, Italy;* orcid.org/0000-0002-3601-7141; Email: piccinin@iom.cnr.it

Authors

Mina Taleblou − *CNR-IOM, Consiglio Nazionale delle Ricerche, Istituto Officina dei Materiali, Trieste 34136, Italy;* orcid.org/0000-0003-2434-461X

Matteo Farnesi Camellone − *CNR-IOM, Consiglio Nazionale delle Ricerche, Istituto Officina dei Materiali, Trieste 34136, Italy;* orcid.org/0000-0001-9180-0115

Stefano Fabris − *CNR-IOM, Consiglio Nazionale delle Ricerche, Istituto Officina dei Materiali, Trieste 34136, Italy;* orcid.org/0000-0003-2562-8788

Complete contact information is available at: https://pubs.acs.org/10.1021/acs.jpcc.3c05714

Notes

The authors declare no competing financial interest.

REFERENCES

(1) Liu, Z.-P.; Hu, P.; Alavi, A. Catalytic Role of Gold in Gold-Based Catalysts: A Density Functional Theory Study on the CO Oxidation on Gold. *J. Am. Chem. Soc.* **2002**, *124*, 14770−14779.

(2) Ha, H.; An, H.; Yoo, M.; Lee, J.; Kim, H. Y. Catalytic CO Oxidation by CO-Saturated Au Nanoparticles Supported on CeO2: Effect of CO Coverage. *J. Phys. Chem. C* **2017**, *121*, 26895−26902.

(3) Kim, H. Y.; Lee, H. M.; Henkelman, G. CO Oxidation Mechanism on CeO2-Supported Au Nanoparticles. *J. Am. Chem. Soc.* **2012**, *134*, 1560−1570.

(4) Chen, B.-R.; Crosby, L. A.; George, C.; Kennedy, R. M.; Schweitzer, N. M.; Wen, J.; Van Duyne, R. P.; Stair, P. C.; Poeppelmeier, K. R.; Marks, L. D.; Bedzyk, M. J. Morphology and CO Oxidation Activity of Pd Nanoparticles on SrTiO3 Nano-polyhedra. *ACS Catal.* **2018**, *8*, 4751−4760.

(5) Sushchikh, M.; Cameron, L.; Metiu, H.; McFarland, E. W. Size and pressure independent kinetics of CO oxidation on alumina-supported iridium nanoparticles. *Int. J. Chem. Kinet.* **2008**, *40*, 826−830.

(6) DeSario, P. A.; Pitman, C. L.; Delia, D. J.; Driscoll, D. M.; Maynes, A. J.; Morris, J. R.; Pennington, A. M.; Brintlinger, T. H.; Rolison, D. R.; Pietron, J. J. Low-temperature CO oxidation at persistent low-valent Cu nanoparticles on TiO2 aerogels. *Appl. Catal., B* **2019**, *252*, 205−213.

(7) Lamoth, M.; Plodinec, M.; Scharfenberg, L.; Wrabetz, S.; Girgsdies, F.; Jones, T.; Rosowski, F.; Horn, R.; Schlögl, R.; Frei, E. Supported Ag Nanoparticles and Clusters for CO Oxidation: Size Effects and Influence of the Silver−Oxygen Interactions. *ACS Appl. Nano Mater.* **2019**, *2*, 2909−2920.

(8) Allian, A. D.; Takanabe, K.; Fujdala, K. L.; Hao, X.; Truex, T. J.; Cai, J.; Buda, C.; Neurock, M.; Iglesia, E. Chemisorption of CO and Mechanism of CO Oxidation on Supported Platinum Nanoclusters. *J. Am. Chem. Soc.* **2011**, *133*, 4498−4517.

(9) Rashkeev, S. N.; Lupini, A. R.; Overbury, S. H.; Pennycook, S. J.; Pantelides, S. T. Role of the nanoscale in catalytic CO oxidation by supported Au and Pt nanostructures. *Phys. Rev. B: Condens. Matter Mater. Phys.* **2007**, *76*, 035438.

(10) Kim, G. J.; Kwon, D. W.; Hong, S. C. Effect of Pt Particle Size and Valence State on the Performance of Pt/TiO2 Catalysts for CO Oxidation at Room Temperature. *J. Phys. Chem. C* **2016**, *120*, 17996−18004.

(11) Song, H. C.; Oh, S.; Kim, S. H.; Lee, S. W.; Moon, S. Y.; Choi, H.; Kim, S.-H.; Kim, Y.; Oh, J.; Park, J. Y. The effect of the oxidation states of supported oxides on catalytic activity: CO oxidation studies on Pt/cobalt oxide. *Chem. Commun.* **2019**, *55*, 9503−9506.

(12) Ruiz Puigdollers, A.; Schlexer, P.; Tosoni, S.; Pacchioni, G. Increasing Oxide Reducibility: The Role of Metal/Oxide Interfaces in the Formation of Oxygen Vacancies. *ACS Catal.* **2017**, *7*, 6493−6513.

(13) Widmann, D.; Krautsieder, A.; Walter, P.; Brückner, A.; Behm, R. J. How Temperature Affects the Mechanism of CO Oxidation on Au/TiO2: A Combined EPR and TAP Reactor Study of the Reactive Removal of TiO2 Surface Lattice Oxygen in Au/TiO2 by CO. *ACS Catal.* **2016**, *6*, 5005−5011.

(14) Liu, L.; Corma, A. Metal Catalysts for Heterogeneous Catalysis: From Single Atoms to Nanoclusters and Nanoparticles. *Chem. Rev.* **2018**, *118*, 4981−5079.

(15) Afanasev, D.; Yakovina, O.; Kuznetsova, N.; Lisitsyn, A. High activity in CO oxidation of Ag nanoparticles supported on fumed silica. *Catal. Commun.* **2012**, *22*, 43−47.

(16) An, N.; Li, S.; Duchesne, P. N.; Wu, P.; Zhang, W.; Lee, J.-F.; Cheng, S.; Zhang, P.; Jia, M.; Zhang, W. Size Effects of Platinum Colloid Particles on the Structure and CO Oxidation Properties of Supported Pt/Fe2O3 Catalysts. *J. Phys. Chem. C* **2013**, *117*, 21254−21262.

(17) Liu, J.-X.; Filot, I. A. W.; Su, Y.; Zijlstra, B.; Hensen, E. J. M. Optimum Particle Size for Gold-Catalyzed CO Oxidation. *J. Phys. Chem. C* **2018**, *122*, 8327−8340.

(18) Clark, P. D.; Sui, R.; Dowling, N. I.; Huang, M.; Lo, J. M. Oxidation of CO in the presence of SO2 using gold supported on La2O3/TiO2 nanofibers. *Catal. Today* **2013**, *207*, 212−219.

(19) Du, X.; Han, W.; Tang, Z.; Zhang, J. Controlled synthesis of Pd/CoOx−InOx nanofibers for low-temperature CO oxidation reaction. *New J. Chem.* **2019**, *43*, 14872−14882.

(20) Qadir, K.; Kim, S. M.; Seo, H.; Mun, B. S.; Akgul, F. A.; Liu, Z.; Park, J. Y. Deactivation of Ru Catalysts under Catalytic CO Oxidation by Formation of Bulk Ru Oxide Probed with Ambient Pressure XPS. *J. Phys. Chem. C* **2013**, *117*, 13108−13113.

(21) Bosio, N.; Di, M.; Skoglundh, M.; Carlsson, P.-A.; Grönbeck, H. Interface Reactions Dominate Low-Temperature CO Oxidation Activity over Pt/CeO2. *J. Phys. Chem. C* **2022**, *126*, 16164−16171.
(22) Cai, Q.; Wang, X.; Wang, J.-g. Distinctions between Supported Au and Pt Catalysts for CO Oxidation: Insights from DFT Study. *J. Phys. Chem. C* **2013**, *117*, 21331−21336.
(23) An, K.; Alayoglu, S.; Musselwhite, N.; Plamthottam, S.; Melaet, G.; Lindeman, A. E.; Somorjai, G. A. Enhanced CO Oxidation Rates at the Interface of Mesoporous Oxides and Pt Nanoparticles. *J. Am. Chem. Soc.* **2013**, *135*, 16689−16696.
(24) Song, J.; Yang, Y.; Liu, S.; Li, L.; Yu, N.; Fan, Y.; Chen, Z.; Kuai, L.; Geng, B. Dispersion and support dictated properties and activities of Pt/metal oxide catalysts in heterogeneous CO oxidation. *Nano Res.* **2021**, *14*, 4841−4847.
(25) Li, N.; Chen, Q.-Y.; Luo, L.-F.; Huang, W.-X.; Luo, M.-F.; Hu, G.-S.; Lu, J.-Q. Kinetic study and the effect of particle size on low temperature CO oxidation over Pt/TiO2 catalysts. *Appl. Catal., B* **2013**, *142*−*143*, 523−532.
(26) Oh, S.; Ha, H.; Choi, H.; Jo, C.; Cho, J.; Choi, H.; Ryoo, R.; Kim, H. Y.; Park, J. Y. Oxygen activation on the interface between Pt nanoparticles and mesoporous defective TiO2 during CO oxidation. *J. Chem. Phys.* **2019**, *151*, 234716.
(27) Heiz, U.; Sanchez, A.; Abbet, S.; Schneider, W.-D. Catalytic Oxidation of Carbon Monoxide on Monodispersed Platinum Clusters: Each Atom Counts. *J. Am. Chem. Soc.* **1999**, *121*, 3214−3217.
(28) Beniya, A.; Miwa, K.; Hirata, H.; Watanabe, Y.; Higashi, S. Insight for Designing Mass-Efficient Metal-Oxide-Supported Heterogeneous Catalyst from the Identification of the Catalytically Active Edge Sites Using Isotopically Labeled 13CO and 18O2. *ACS Catal.* **2022**, *12*, 1977−1985.
(29) Thang, H. V.; Pacchioni, G. CO Oxidation Promoted by a Pt4/TiO2 Catalyst: Role of Lattice Oxygen at the Metal/Oxide Interface. *Catal. Lett.* **2019**, *149*, 390−398.
(30) DeRita, L.; Dai, S.; Lopez-Zepeda, K.; Pham, N.; Graham, G. W.; Pan, X.; Christopher, P. Catalyst Architecture for Stable Single Atom Dispersion Enables Site-Specific Spectroscopic and Reactivity Measurements of CO Adsorbed to Pt Atoms, Oxidized Pt Clusters, and Metallic Pt Clusters on TiO2. *J. Am. Chem. Soc.* **2017**, *139*, 14150−14165.
(31) Peña-Torres, A.; Ali, A.; Stamatakis, M.; Jónsson, H. Indirect mechanism of Au adatom diffusion on the Si(100) surface. *Phys. Rev. B* **2022**, *105*, 205411.
(32) Liang, J.-X.; Lin, J.; Yang, X.-F.; Wang, A.-Q.; Qiao, B.-T.; Liu, J.; Zhang, T.; Li, J. Theoretical and Experimental Investigations on Single-Atom Catalysis: Ir_1/FeO_x for CO Oxidation. *J. Phys. Chem. C* **2014**, *118*, 21945−21951.
(33) Qiao, B.; Wang, A.; Yang, X.; Allard, L.; Jiang, Z.; Cui, Y.; Liu, J.; Li, J.; Zhang, T. Single-atom catalysis of CO oxidation using Pt1/FeOx. *Nat. Chem.* **2011**, *3*, 634−641.
(34) Liang, J.; Yang, X.; Xu, C.; Zhang, T.; Li, J. Catalytic ativities of single-atom catalysts for CO oxidation: Pt1/FeOx vs. Fe1/FeOx. *Chin. J. Catal.* **2017**, *38*, 1566−1573.
(35) Kistler, J. D.; Chotigkrai, N.; Xu, P.; Enderle, B.; Praserthdam, P.; Chen, C.-Y.; Browning, N. D.; Gates, B. C. A Single-Site Platinum CO Oxidation Catalyst in Zeolite KLTL: Microscopic and Spectroscopic Determination of the Locations of the Platinum Atoms. *Angew. Chem., Int. Ed.* **2014**, *53*, 8904−8907.
(36) Lin, H.; Li, L.; Zhao, M.; Huang, X.; Chen, X.; Li, G.; Yu, R. Synthesis of High-Quality Brookite TiO2 Single-Crystalline Nanosheets with Specific Facets Exposed: Tuning Catalysts from Inert to Highly Reactive. *J. Am. Chem. Soc.* **2012**, *134*, 8328−8331.
(37) Zhao, W.; Li, Y.; Shen, W. Tuning the shape and crystal phase of TiO2 nanoparticles for catalysis. *Chem. Commun.* **2021**, *57*, 6838−6850.
(38) Gong, X.-Q.; Selloni, A. First-principles study of the structures and energetics of stoichiometric brookite TiO_2 surfaces. *Phys. Rev. B: Condens. Matter Mater. Phys.* **2007**, *76*, 235307.
(39) Meyer, W.; Biedermann, K.; Gubo, M.; Hammer, L.; Heinz, K. Surface structure of polar Co3O4(111) films grown epitaxially on Ir(100)-(1 × 1). *J. Phys.: Cond. Matt.* **2008**, *20*, 265011.
(40) Lykhach, Y.; Piccinin, S.; Skála, T.; Bertram, M.; Tsud, N.; Brummel, O.; Farnesi Camellone, M.; Beranová, K.; Neitzel, A.; Fabris, S.; et al. Quantitative Analysis of the Oxidation State of Cobalt Oxides by Resonant Photoemission Spectroscopy. *J. Phys. Chem. Lett.* **2019**, *10*, 6129−6136.
(41) Giannozzi, P.; Baroni, S.; Bonini, N.; Calandra, M.; Car, R.; Cavazzoni, C.; Ceresoli, D.; Chiarotti, G. L.; Cococcioni, M.; Dabo, I.; et al. QUANTUM ESPRESSO: a Modular and Open-source Software Project for Quantum Simulations of Materials. *J. Phys.: Condens. Matter* **2009**, *21*, 395502.
(42) Perdew, J. P.; Burke, K.; Ernzerhof, M. Generalized Gradient Approximation Made Simple. *Phys. Rev. Lett.* **1996**, *77*, 3865−3868.
(43) Cheng, H.; Selloni, A. Energetics and diffusion of intrinsic surface and subsurface defects on anatase TiO2(101). *J. Chem. Phys.* **2009**, *131*, 054703.
(44) Taleblou, M.; Camellone, M. F.; Fabris, S.; Piccinin, S. Oxidation of Gas-Phase and Supported Pt Nanoclusters: An Ab Initio Investigation. *J. Phys. Chem. C* **2022**, *126*, 10880−10888.
(45) Reuter, K.; Scheffler, M. Composition, Structure, and Stability of $RuO_2(110)$ as a Function of Oxygen Pressure. *Phys. Rev. B: Condens. Matter Mater. Phys.* **2001**, *65*, 035406.
(46) Thomas, C. A. *NIST-JANAF Thermochemical Tables—SRD 13*, 2013.
(47) Chen, H.-Y. T.; Tosoni, S.; Pacchioni, G. Adsorption of Ruthenium Atoms and Clusters on Anatase TiO2 and Tetragonal ZrO2(101) Surfaces: A Comparative DFT Study. *J. Phys. Chem. C* **2015**, *119*, 10856−10868.
(48) Sheppard, D.; Terrell, R.; Henkelman, G. Optimization methods for finding minimum energy paths. *J. Chem. Phys.* **2008**, *128*, 134106.
(49) Li, Z.; Geng, Y.; Ma, L.; Chen, X.; Li, J.; Chang, H.; Schwank, J. W. Catalytic oxidation of CO over Pt/Fe3O4 catalysts: Tuning O2 activation and CO adsorption. *Front. Environ. Sci. Eng.* **2020**, *14*, 65.
(50) Ferrari, P.; Molina, L. M.; Kaydashev, V. E.; Alonso, J. A.; Lievens, P.; Janssens, E. Controlling the Adsorption of Carbon Monoxide on Platinum Clusters by Dopant-Induced Electronic Structure Modification. *Angew. Chem., Int. Ed.* **2016**, *55*, 11059−11063.
(51) Demirdjian, B.; Ozerov, I.; Bedu, F.; Ranguis, A.; Henry, C. R. CO and O_2 Adsorption and CO Oxidation on Pt Nanoparticles by Indirect Nanoplasmonic Sensing. *ACS Omega* **2021**, *6*, 13398−13405.
(52) Bliem, R.; van der Hoeven, J. E. S.; Hulva, J.; Pavelec, J.; Gamba, O.; de Jongh, P. E.; Schmid, M.; Blaha, P.; Diebold, U.; Parkinson, G. S. Dual role of CO in the stability of subnano Pt clusters at the Fe_3O_4 (001) surface. *Proc. Natl. Acad. Sci. U.S.A.* **2016**, *113*, 8921−8926.
(53) Blackman, G. S.; Xu, M. L.; Ogletree, D. F.; Van Hove, M. A.; Somorjai, G. A. Mix of Molecular Adsorption Sites Detected for Disordered CO on Pt(111) by Diffuse Low-Energy Electron Diffraction. *Phys. Rev. Lett.* **1988**, *61*, 2352−2355.
(54) Kalhara Gunasooriya, G. T. K.; Saeys, M. CO Adsorption Site Preference on Platinum: Charge Is the Essence. *ACS Catal.* **2018**, *8*, 3770−3774.
(55) Liu, F.; Wu, C.; Yang, G.; Yang, S. CO Oxidation over Strained Pt(100) Surface: A DFT Study. *J. Phys. Chem. C* **2015**, *119*, 15500−15505.
(56) Paz-Borbon, L. O.; Johnston, R. L.; Barcaro, G.; Fortunelli, A. Chemisorption of CO and H on Pd, Pt and Au nanoclusters: a DFT approach. *Eur. Phys. J. D* **2009**, *52*, 131−134.
(57) Sangnier, A.; Genty, E.; Iachella, M.; Sautet, P.; Raybaud, P.; Matrat, M.; Dujardin, C.; Chizallet, C. Thermokinetic and Spectroscopic Mapping of Carbon Monoxide Adsorption on Highly Dispersed Pt/-Al2O3. *ACS Catal.* **2021**, *11*, 13280−13293.
(58) Singh, J.; Nelson, R. C.; Vicente, B. C.; Scott, S. L.; van Bokhoven, J. A. Electronic structure of alumina-supported mono-

https://doi.org/10.1021/acs.jpcc.3c05714
J. Phys. Chem. C 2023, 127, 21132−21149

metallic Pt and bimetallic PtSn catalysts under hydrogen and carbon monoxide environment. *Phys. Chem. Chem. Phys.* **2010**, *12*, 5668.
(59) Ghosh, P.; Farnesi Camellone, M.; Fabris, S. Fluxionality of Au Clusters at Ceria Surfaces during CO Oxidation: Relationships among Reactivity, Size, Cohesion, and Surface Defects from DFT Simulations. *J. Phys. Chem. Lett.* **2013**, *4*, 2256−2263.
(60) Zhai, H.; Alexandrova, A. N. Fluxionality of Catalytic Clusters: When It Matters and How to Address It. *ACS Catal.* **2017**, *7*, 1905−1911.
(61) Lavroff, R. H.; Morgan, H. T.; Zhang, Z.; Poths, P.; Alexandrova, A. N. Ensemble representation of catalytic interfaces: soloists, orchestras, and everything in-between. *Chem. Sci.* **2022**, *13*, 8003−8016.
(62) Baxter, E. T.; Ha, M.-A.; Cass, A. C.; Alexandrova, A. N.; Anderson, S. L. Ethylene Dehydrogenation on Pt4,7,8 Clusters on Al2O3: Strong Cluster Size Dependence Linked to Preferred Catalyst Morphologies. *ACS Catal.* **2017**, *7*, 3322−3335.
(63) Zhou, H.; Chen, X.; Wang, J. CO oxidation over supported Pt clusters at different CO coverage. *Int. J. Quantum Chem.* **2016**, *116*, 939−944.
(64) Lu, Y.; Thompson, C.; Kunwar, D.; Datye, A. K.; Karim, A. M. Origin of the High CO Oxidation Activity on CeO2 Supported Pt Nanoparticles: Weaker Binding of CO or Facile Oxygen Transfer from the Support? *ChemCatChem* **2020**, *12*, 1726−1733.
(65) Reuter, K.; Scheffler, M. Composition and structure of the RuO_2(110) surface in an O_2 and CO environment: Implications for the catalytic formation of CO_2. *Phys. Rev. B: Condens. Matter Mater. Phys.* **2003**, *68*, 045407.
(66) Beniya, A.; Higashi, S.; Ohba, N.; Jinnouchi, R.; Hirata, H.; Watanabe, Y. CO oxidation activity of non-reducible oxide-supported mass-selected few-atom Pt single-clusters. *Nat. Commun.* **2020**, *11*, 1888.
(67) Liu, H.-H.; Wang, Y.; Jia, A.-P.; Wang, S.-Y.; Luo, M.-F.; Lu, J.-Q. Oxygen vacancy promoted CO oxidation over Pt/CeO2 catalysts: A reaction at Pt−CeO2 interface. *Appl. Surf. Sci.* **2014**, *314*, 725−734.
(68) Kaiser, S.; Maleki, F.; Zhang, K.; Harbich, W.; Heiz, U.; Tosoni, S.; Lechner, B. A. J.; Pacchioni, G.; Esch, F. Cluster Catalysis with Lattice Oxygen: Tracing Oxygen Transport from a Magnetite (001) Support onto Small Pt Clusters. *ACS Catal.* **2021**, *11*, 9519−9529.
(69) Maynes, A. J.; Driscoll, D. M.; DeSario, P. A.; Pietron, J. J.; Pennington, A. M.; Rolison, D. R.; Morris, J. R. Electronic Metal−Support Interactions in the Activation of CO Oxidation over a Cu/TiO2 Aerogel Catalyst. *J. Phys. Chem. C* **2020**, *124*, 21491−21501.
(70) Schlexer, P.; Widmann, D.; Behm, R. J.; Pacchioni, G. CO Oxidation on a Au/TiO_2 Nanoparticle Catalyst via the Au-Assisted Mars−van Krevelen Mechanism. *ACS Catal.* **2018**, *8*, 6513−6525.
(71) Matsui, T.; Kamiuchi, N.; Fujiwara, K.; Kikuchi, R.; Eguchi, K. Electrochemical CO Oxidation and Microstructure in Pt/Co[sub 3]O[sub 4]-Based Catalysts. *J. Electrochem. Soc.* **2009**, *156*, K128.
(72) Wang, L.; Deo, S.; Mukhopadhyay, A.; Pantelis, N. A. I.; Janik, M. J.; Rioux, R. M. Emergent Behavior in Oxidation Catalysis over Single-Atom Pd on a Reducible CeO2 Support via Mixed Redox Cycles. *ACS Catal.* **2022**, *12*, 12927−12941.
(73) Bac, S.; Mallikarjun Sharada, S. CO Oxidation with Atomically Dispersed Catalysts: Insights from the Energetic Span Model. *ACS Catal.* **2022**, *12*, 2064−2076.
(74) Qin, Y.-Y.; Su, Y.-Q. A DFT Study on Heterogeneous Pt/CeO2(110) Single Atom Catalysts for CO Oxidation. *ChemCatChem* **2021**, *13*, 3857−3863.
(75) Su, Y.-Q.; Wang, Y.; Liu, J.-X.; Filot, I. A.; Alexopoulos, K.; Zhang, L.; Muravev, V.; Zijlstra, B.; Vlachos, D. G.; Hensen, E. J. Theoretical Approach To Predict the Stability of Supported Single-Atom Catalysts. *ACS Catal.* **2019**, *9*, 3289−3297.
(76) Tang, Y.; Wang, Y.-G.; Li, J. Theoretical Investigations of Pt1@CeO2 Single-Atom Catalyst for CO Oxidation. *J. Phys. Chem. C* **2017**, *121*, 11281−11289.
(77) Wang, H.; Liu, J.-X.; Allard, L. F.; Lee, S.; Liu, J.; Li, H.; Wang, J.; Wang, J.; Oh, S. H.; Li, W.; et al. Surpassing the single-atom catalytic activity limit through paired Pt-O-Pt ensemble built from isolated Pt1 atoms. *Nat. Commun.* **2019**, *10*, 3808.
(78) Wang, X.; Zhang, L.; Bu, Y.; Sun, W. Interplay between invasive single atom Pt and native oxygen vacancy in rutile TiO2(110) surface: A theoretical study. *Nano Res.* **2022**, *15*, 669−676.
(79) Lou, Y.; Liu, J. CO Oxidation on Metal Oxide Supported Single Pt atoms: The Role of the Support. *Ind. Eng. Chem. Res.* **2017**, *56*, 6916−6925.
(80) Hoang, S.; Guo, Y.; Binder, A. J.; Tang, W.; Wang, S.; Liu, J. J.; Tran, H.; Lu, X.; Wang, Y.; Ding, Y.; et al. Activating low-temperature diesel oxidation by single-atom Pt on TiO2 nanowire array. *Nat. Commun.* **2020**, *11*, 1062.
(81) García-Diéguez, M.; Iglesia, E. Structure sensitivity via decoration of low-coordination exposed metal atoms: CO oxidation catalysis on Pt clusters. *J. Catal.* **2013**, *301*, 198−209.
(82) Moses-DeBusk, M.; Yoon, M.; Allard, L. F.; Mullins, D. R.; Wu, Z.; Yang, X.; Veith, G.; Stocks, G. M.; Narula, C. K. CO Oxidation on Supported Single Pt Atoms: Experimental and ab Initio Density Functional Studies of CO Interaction with Pt Atom on -Al2O3 (010) Surface. *J. Am. Chem. Soc.* **2013**, *135*, 12634−12645.
(83) Gao, H. CO oxidation mechanism on the -Al2O3 supported single Pt atom: First principle study. *Appl. Surf. Sci.* **2016**, *379*, 347−357.
(84) Bligaard, T.; Nørskov, J.; Dahl, S.; Matthiesen, J.; Christensen, C.; Sehested, J. The Brønsted−Evans−Polanyi relation and the volcano curve in heterogeneous catalysis. *J. Catal.* **2004**, *224*, 206−217.

https://doi.org/10.1021/acs.jpcc.3c05714
J. Phys. Chem. C 2023, 127, 21132−21149